VITAL SIGNS MONITORING USING ULTRA WIDE BAND PULSE RADAR

RELATORE: Dr. S. Tomasin

LAUREANDO: Luigi Di Lena

CORSO DI LAUREA IN: Ingegneria delle Telecomunicazioni

A.A. 2009-2010

UNIVERSITÀ DEGLI STUDI DI PADOVA
DIPARTIMENTO DI INGEGNERIA DELL'INFORMAZIONE
TESI DI LAUREA

VITAL SIGNS MONITORING USING ULTRA WIDE BAND PULSE RADAR

RELATORE: Dr. S. Tomasin

LAUREANDO: *Luigi Di Lena*

Padova, 4 ottobre 2010

”Stay Hungry. Stay Foolish.”
Steve Jobs - Apple

Contents

Abstract

The aim of this work is to describe how to realize a measurement setup to detect target heart and breath rate with the use of Ultra Wide Band (UWB) radar technology. Thanks to UWB wireless capabilities the detection is done contactless just standing still at a given distance d_T. Contactless heart and breath rate detection can be achieved with the use of currently available commercial UWB radar devices. This is of interest for intensive-care patient monitoring, home monitoring, fast disease screening and remote vital signs monitoring. Our setup is composed by devices provided by PulsON: two PulsON 220RD UWB radars. We encountered an issue with time synchronization that is very critical in UWB detection techniques and therefore a custom built synchronization algorithm has been developed trying to automatically resynchronize the scan. The algorithm does the job but can not fully cope with the out-of-sync issue resulting in an big amount of scans not being selected due to very high Mean Square Error (MSE) value. Then, thanks to a vital sign dataset taken without any issue with a previous PulsON device - 210 RD - we analyze and propose two different order FIR filters to enhance heart beat period detection. Both filters are pass band that cut everything outside average healthy adult heart rate range of $50 - 120$ beat per minute (bpm) and amplify a bit the inside range. Heart rate detection is then performed with the help of three of the most well known period detection algorithms: Welch algorithm, MUltiple Sgnal Classification (MUSIC) algorithm and Average Magnitude Difference Function (AMDF) technique. A low complexity version of the maximum likelihood technique is also introduced. The double filter solution aims to get the best from all the period detection algorithms. Finally, a comparison between all these algorithms shows that the maximum likelihood algorithm approach is the best performing without any signal processing. The double filter order approach does not get the desired effect and the higher order is then chosen. After applying the 70-th order designed filter we have an overall improvement except for PWELCH and MUSIC algorithms.

Chapter 1

Introduction

This work describes how to realize a measurement setup to detect target heart and breath rate with the use of Ultra Wide Band (UWB) radar technology. Thanks to UWB wireless capabilities the detection is done contactless just standing still at a known distance. This is of interest for intensive-care patient monitoring, home monitoring, fast disease screening and also remote vital signs monitoring. In Chapter 2, after a short overview about the state of art of UWB technology, we will discuss on contactless heart and breath rate detection that can be achieved with the use of currently available commercial UWB radar devices. In the same chapter is presented a human body dielectric characterization and the UWB model used in the setup. Section 2.3.4 shows in depth how to remove static component, known as background noise, from the received data signal to get just the oscillating part. Our measurement setup is composed by two PulsON 220 RD UWB radar, their emission measurements and specifications are covered in Chapter 3 also with a brief description of the bistatic radar application and a full explanation of the parameters involved in it. Working with the PulsON 220 RD we face a very difficult challenge regarding signal synchronization; the device output is completely out-of-sync and there is no option or tweak to solve this issue. A script solution is proposed and analyzed in Section 3.2.2, unfortunately the problem can not be solved via software. Next, we continue our work on a vital sign dataset taken with the previous PulsON 210 RD devices unaffected by the out-of-sync issue. The provided data contains a real scenario data acquisition. In Chapter 4 we will cover signal processing operated by the devices and the necessary filters we need to apply in order to proceed with the vital signs period

detection. Period detection is made possible with the help of four detection algorithms. Section 4.2 presents these and also their performance comparison. Keeping in mind that the received data is made up of both heart and breath component we want to enhance the first being also the weaker. The idea behind filter design is presented in Section 4.2.9 where two different filters are designed and compared to find the best performing with the lowerer possible order. Finally, Chapter 5 sums up our efforts to detect vital signs via contactless UWB radar coping with the out-of-sync issue. The best performing Finite Impulse Response (FIR) filter for heart beat enhancement is proposed as result of a two way design comparison.

Chapter 2

Ultra Wide Band

2.1 Overview

Ultra Wide Band (UWB) is a technology for transmitting information spread over a large bandwidth (> 500 MHz) that should, in theory and under the right circumstances, be able to share spectrum with other users. Regulatory settings of Federal Communications Commission (FCC) are intended to provide an efficient use of scarce radio bandwidth while enabling high data rate "personal area network" (PAN) wireless connectivity and longer-range, low data rate applications and radar and imaging systems. UWB was traditionally accepted as pulse radio, but the FCC and International Telecommunication Union Radiocommunication Sector (ITU-R) now define UWB in terms of a transmission from an antenna for which the emitted signal bandwidth exceeds the minimum between 500 MHz and 20% of the center frequency. Thus, pulse-based systems wherein each transmitted pulse instantaneously occupies the UWB bandwidth, or an aggregation of at least 500 MHz worth of narrow band carriers, for example in orthogonal frequency-division multiplexing (OFDM) can gain access to the UWB spectrum. Pulse repetition rates may be either low or very high. Pulse-based UWB radars and imaging systems tend to use low repetition rates, typically in the range of 1 to 100 megapulses per second. On the other hand, communications systems favor high repetition rates, typically in the range of 1 to 2 giga-pulses per second, thus enabling short-range gigabit-per-second communications systems. Each pulse in a pulse-based UWB system occupies the entire UWB bandwidth, thus reaping the benefits of relative immunity to multipath fading (but not to intersymbol

interference), unlike carrier-based systems that are subject to both deep fades and intersymbol interference.

A significant difference between traditional radio transmissions and UWB radio transmissions is that traditional systems transmit information by varying the power level, frequency, and/or phase of a sinusoidal wave. UWB transmissions instead transmit information by generating radio energy at specific time instants and occupying large bandwidth thus enabling both pulse-position and time-modulation. The information can also be modulated on UWB pulses by encoding the polarity of the pulse, the amplitude of the pulse, and/or by using orthogonal pulses. UWB pulses can be sent sporadically at relatively low pulse rates to support time/position modulation, but can also be sent at rates up to the inverse of the UWB pulse bandwidth. Pulse UWB systems have been demonstrated at channel pulse rates in excess of 1.3 giga-pulses per second using a continuous stream of UWB pulses (Continuous Pulse UWB or "C-UWB"), supporting forward error correction encoded data rates in excess of 675 Mbit/s. Such a pulse-based UWB method using bursts of pulses is the basis of the IEEE 802.15.4a draft standard and working group, which has proposed UWB as an alternative physical layer. One of the valuable aspects of UWB radio technology is the ability to determine the "time of flight" of the direct path of the radio transmission between the transmitter and receiver at various frequencies. Another valuable aspect of pulse-based UWB is that the pulses are very short in space (less than 60 cm for a 500 MHz wide pulse, less than 23 cm for a 1.3 GHz bandwidth pulse).

Due to the extremely low emission levels currently allowed by regulatory agencies, UWB systems tend to be short-range and indoors applications. However, due to the short duration of the UWB pulses, it is easier to engineer extremely high data rates, and data rate can be readily traded for range by simply aggregating pulse energy per data bit using either simple integration or by coding techniques. Conventional OFDM technology can also be used subject to the minimum bandwidth requirement of the regulations. High data rate UWB can enable wireless monitors, the efficient transfer of data from digital camcorders, wireless printing of digital pictures from a camera without the need for an intervening personal computer, and the transfer of files among cell phone handsets and other handheld devices like personal digital audio and video players. UWB is used as a

part of realtime location systems. The precision capabilities combined with the very low power make it ideal for certain radio frequency sensitive environments such as hospitals and health care. U.S.-based Parco Merged Media Corporation was the first system developer to deploy a commercial version of this system in a Washington, DC hospital. UWB is also used in "see-through-the-wall" precision radar imaging technology, precision locating and tracking (using distance measurements between radios), and precision time-of-arrival-based localization approaches. It exhibits excellent efficiency with a spatial capacity of approximately $10^{13} bit/s/m^2$. UWB has been proposed as technology for use in personal area networks and appeared in the IEEE 802.15.3a draft PAN standard. However, after several years of deadlock, the IEEE 802.15.3a task group was dissolved in 2006. Slow progress in UWB standards development, high cost of initial implementations and performance significantly lower than initially expected are some of the reasons for the limited success of UWB in consumer products, which caused several UWB vendors to cease operations during 2008 and 2009.

2.2 Survey of UWB state of the art

2.2.1 UWB impulse radars as biomedical sensors

UWB radar technology has been first researched by US Army and therefore much of it is classified. This technology applies in several fields such as terrain profiling through foliage or camouflage and ground penetration to find buried objects or people. Those applications were such appealing that in 1990 the US Defense Advance Research Projects Agency (DARPA) commissioned a study to verify them. The idea of human vital signs monitoring via UWB radar started in the early 1970s but was soon hindered by its cost for the time. One of the first US patent regarding medical application of UWB radar is the one awarded to Thomas McEwan. The patent is the result of work done by the US Lawrence Livermore National Laboratory.

The publication is about promising medical applications of the technology and it emphasizes that the average emission level ($\approx 1\mu W$) is three orders of magnitude lower than most international standard requirements for continuous human exposure to microwaves thus making the device medically harmless. UWB radar applications in medicine are being or were studied at University of California

Davis, University of California Berkeley, University of Iowa and a fee experimental prototypes where built and tested also by Tor Vergata University of Rome. This last reference is very interesting because it is the first attempt to model the phenomena of UWB pulse scattering along the path to the heart. However, up to now, no commercial device has hit the market.
We could compare UWB with ultrasound. Although UWB and ultrasound are in fact very similar and many of the signal processing techniques used in ultrasonic systems can be applied to UWB systems, it is different from ultrasound which has broad application in today's world. The major difference is that ultrasound is basically a line of sight technology and it is very short range since it is used for medical imaging but it typically works only over a few inches. However, UWB is different because it does not use high frequency sound waves which can not penetrate obstacles. This makes UWB viable for wide area applications where obstacles are certain to be encountered, although ultrasound may also be inoperable in these circumstances [1]. The feature makes it easy to monitor organs of the human body for medical application.

2.2.2 UWB communications

UWB communications are regarded as the future high data rate and short range transmission technology. Since late 2001 the IEEE Wireless Personal Area Networks Groups started a standardization process, that has received a lot of contributions and research resources from academy and private companies.
The first applications providing a complete chip-set solution (i.e. Medium Access Controller, Baseband controller and Radio Frequency receiver) are hitting the market. This proves that, even though the technology has not yet been standardized, it is maturing quickly.

2.2.3 Radar and communications integration

The integration of radar sensing together with communications equipment has been used in aerospace satellites and exploration vehicles mainly in order to save space, since some components such as the transmitter, receiver and antenna can perform well in either role. Example of such integration made possible is the NASA's Space Shuttle Orbiter [2]. This *ku* band system integrates a wideband

two-way data system and a frequency-hopping, low repetition rate, pulse-Doppler radar. In radar mode the system measures range, velocity, angle and angle rate; in communication mode, it receives and demodulates the spread spectrum forward and return link with ground station. Frequency diversity is used to integrate both systems assigning a band of 13.775 GHz for communications and a band of 13.8∼14.0 GHz for radar.
Not only NASA was interested in this kind of integration: Mazda Motor Corp. presented a vehicle-to-vehicle communication and ranging system based on the ranging capabilities of spread spectrum. A car equipped with this system can range other not equipped cars by measuring the start of the returned Pseudo-Noise code as given by the correlation peak. The maximum achieved range between cars was about 1 meter and the maximum achievable date rate was about 12.6 kbps.

2.2.4 Regulations

Any new medical monitoring system must comply with actual legislation on electromagnetical emissions hence the only way for UWB systems to reach large scale usage is to be designed with emissions in mind. Currently, the most widely known emission masks for UWB radio are those issued by FCC in the US [3]. The FCC's regulation established three types of UWB devices based on their potential to cause interference: 1) imaging systems including Ground Penetrating Radars (GPRs); wall-through-wall surveillance, and medical imaging devices, 2) vehicular radar systems, and 3) communications and measurement systems. The regulation says that medical systems must operate in the 3.1∼10.6 GHz frequency band and describes it as a system that *"may be used for a variety of health applications to 'see' inside the body of a person or animal"*.
About communications, such as high-speed home and business networking devices, it also sets the range of frequencies between 3.1∼10.6 GHz, thus allowing simultaneous operation of radar sensing and communications inside the same band, which is the interest of this application. In that range, the average power spectral density should not go over -41.3 dBm/MHz in either operation mode.
Finally, in March 2005 the FCC granted a waiver which basically enables the usage of direct sequence UWB as gated system to achieve a power spreading effect similar to frequency hopping. This means gated UWB system can also

transmit at higher power levels and then sit quiet, as long as they still meet the same limits for average power density during the certification testing. The waiver means a) higher data rates while using communication UWB capability and b) better range while using UWB in the radar mode.

2.3 System model

As an emerging technology combined with its low emission level, UWB wireless communication provides a very different approach to wireless technologies compared to conventional narrow band systems, which brings huge research interests in it. UWB has some unique attractive features which are combined with researches in other fields such as wireless communications, radar, and medical engineering fields. Because of this, UWB has still many potential applications to be investigated. One of the promising application areas is medicine. Some unique features of UWB make it very suitable for medical applications. In this work, we will focus on one of its current major medical application such as vital signs monitoring. Because of the highly intense pulses used in UWB technology, it is possible to use UWB radar in medical field for remote monitoring and measuring the patients' motion in short distance. This monitoring function could be applied in intensive care units, emergency rooms, home health care, pediatric clinics (to alert for the Sudden Infant Death Syndrome, SIDS [4]), rescue operations (to look for some heart beating under ruins, or soil, or snow). UWB monitoring of respiratory movement in emergency rooms [5] or intensive care units will be attractive and save much cost especially for large-scale hospitals. Some other typical vital sign monitoring application of UWB include the cardiology system, pneumology system, neurology system and etc. There are increasing requirements for the vital sign monitoring applications of UWB, for example, health monitoring for the old people. The deployment of UWB vital signs monitoring system will enable proactive home monitoring of the patients, which in an aging population could decrease the cost of health care by moving some amount of eligible patients from hospital to home, and keep the home monitoring UWB system connecting to the central controlled surveillant center run in the hospital. To accomplish this goal, we require not only monitoring but also the transmission of the data. This work will focus on heart and breath rate detection and enhancement with a commercial

UWB radar device.

2.3.1 Human body

Heart beating The heart is a muscular organ responsible of pumping blood throughout the blood vessels by repeated, rhythmic contractions. The heart's rhythmic contractions occur spontaneously, although the contraction rate is influenced by nervous or hormonal activity, exercise and emotions. The rhythmic sequence of contractions is coordinated by sinoatrial (SA) and atrioventricular (AV) nodes. The SA note is located in the upper wall of the right atrium and is responsible for the electrical stimulation that starts atrial contraction by creating an action potential. The wave reaches then the AV node in the lower right atrium, where it is delayed to allow enough time for all of the blood in the atria to fill their respective ventricles, and then propagates, leading to a contraction of the ventricles [6]. Due to these electrical signals, atria and ventricles alternately contract and relax in a rhythmic cycle; a single cycle begins and ends with atria and ventricles relaxed.

Respiration Respiration is a complex physiological process whose aim is to ensure both the proper income of oxygen and the disposal of dangerous gases, in particular carbon dioxide, resulting from the cellular respiration process. The amount of oxygen required, and consequently, of waste respiration products to be ejected, is determined by body conditions: physical features (age, gender, weight, ...), current activities and feelings. The frequency of the respiration cycle, denoted as *respiration rate*, and the deepness of breathing, the amount of air inhaled per cycle, is influenced by body conditions but also by external conditions (e.g. air pressure) and by conscious control. In general, respiration is not a stationary process; in fact, parameters as duration, deepness, proportion inspiration/expiration periods, in general change from one cycle to another [7].

Respiration and Heart beating interaction Generally speaking heart beating is influenced by respiration [8]; a close nonlinear coupling exists between the respiratory and cardiovascular systems. Both heart beating and respiration are modified by the target activity; in other words, the target state introduces a correlation between the two processes.

Human body can be viewed as a dielectric with characteristics that vary according to the incident wave frequency [9]. Human skin exhibits phenomena which also contribute to its permittivity such as ability to support current flow and molecular polarization. The electromagnetic wave propagation in dielectric media suffers from the attenuation and for this reason the conductivity of the dielectric is complex [10], i.e.

$$\varepsilon = \varepsilon^{'} - j\varepsilon^{''}, \tag{2.1}$$

where $\varepsilon^{'}$ is the relative permittivity of the biological tissue and $\varepsilon^{''}$ the out-of-phase loss factor associated with it such that

$$\varepsilon^{''} = \frac{\sigma_c}{\varepsilon_0 \omega}, \tag{2.2}$$

where ω is the radiant frequency, ε_0 is the free space permittivity and σ_c is the relative conductivity. The propagation constant γ can be written as $\gamma = \alpha + j\beta$ where the attenuation constant α and the propagation constant β can be written as follows [11]:

$$\alpha_h = \omega \sqrt{\frac{\mu_0 \varepsilon_0 \varepsilon_r}{2}} \left[\sqrt{1 + \left(\frac{\sigma_c}{\omega \varepsilon_0 \varepsilon_r} \right)^2} - 1 \right]^{1/2} \tag{2.3}$$

$$\beta_h = \omega \sqrt{\frac{\mu_0 \varepsilon_0 \varepsilon_r}{2}} \left[\sqrt{1 + \left(\frac{\sigma_c}{\omega \varepsilon_0 \varepsilon_r} \right)^2} + 1 \right]^{1/2}, \tag{2.4}$$

where μ_0 is the free space electromagnetic permeability and ε_r is the relative permittivity. The maximum achievable skin depth is given by $1/\alpha_h$ [11]. Fat and bone have a very low water content and therefore significantly a high depth of penetration. Most other body tissues have a very high water content and for this reasons they have a lesser depth.

2.3.2 UWB model

We consider an Impulsive Radio - Ultra Wide band system for detection of vital signs, where the transmitter and the receiver are on two different blocks (bistatic scenario), and receiving antennas are omnidirectional, for an isotropic signal propagation. The transmitted signal $t(t)$ is a periodic repetition of a unitary energy UWB pulse wave $p(t)$, well known by the receiver, i.e.

$$t(t) = \sum_{n=-\infty}^{+\infty} p(t - nT_S)\cos(2\pi f_C t + \phi_0), \tag{2.5}$$

where $p(t)$ is the UWB pulse wave with duration T_P, f_C is the central frequency, T_S is the pulse repetition period and ϕ_0 is an offset. The received signal

$$y(t) = \int_{-\infty}^{+\infty} h(t,\tau)t(t-\tau)\,d\tau + \eta(t) \tag{2.6}$$

is the sum of the convolution between the transmitted signal $t(t)$ and the channel impulse response $h(t,\tau)$ which includes the indoor channel paths and the effects of target (attenuation, reflections, movements, respiration and heart beating) and the zero mean additive white Gaussian noise with power σ_η^2. The channel impulse response includes a static part, describing all the indoor scatterers and a time variant component effect of the target; time variance is the result of target chest motion according to respiration and heart beating.

We consider an indoor environment where the target is still at a known distance d_T from radar devices (see Fig. 2.1). The target chest is supposed to be in front of the radar device in a line of sight configuration.

Therefore, we focus on the time-varying channel impulse response $h_T(t,\tau)$ due to the target chest movement. According to the spherical waves propagation model, it can be shown that the receiver collects the signal reflected by a small area around the chest center. In fact, the waves reflected at the borders do not reach the receiver antenna in our configuration. This motivates the approximation of the chest as planar surface, moving according to a rigid translation: the reflected waves differ slightly in phase, because of small path length differences from each point of the surface. The target channel impulse response is then a single tap, resulting from the sum of all contributions by the surface points; amplitude α, phase β and Time of Arrival (ToA) τ_T of the channel tap are affected by time variance due to chest motion. Therefore we can consider the target as a single scatterer reflecting the radar signal to the receiver, i.e.

$$h_T(t,\tau) = \alpha e^{j\beta}\delta(\tau - \tau_T), \tag{2.7}$$

where α and β are those in (2.3) and (2.4) and are in general time varing and $\delta(\tau)$ is a kronecker pulse. To characterize the time variance of $h_T(t,\tau)$, we model the chest motion as a linear combination of the oscillations $x_r(t)$, due to respiration,

and $x_h(t)$, due to heart beating, i.e.

$$x(t) = x_r(t) + \xi x_h(t), \tag{2.8}$$

where ξ is the attenuation parameter which underlines the weakness of the heart beating signal on the chest with respect to the respiration signal. We define $R_s(t)$ as the distance covered by radar signal from the transmitter to the receiver through the reflection on target chest. In our scenario, with the assumption of normal incidence on chest surface, we have

$$R_s(t) \approx 2d_T + 2x(t), \tag{2.9}$$

where d_T is the distance between the UWB radar and the chest. $R_s(t)$ is strictly related to target physical condition, age and activity of the target.

2.3.3 Measurement setup

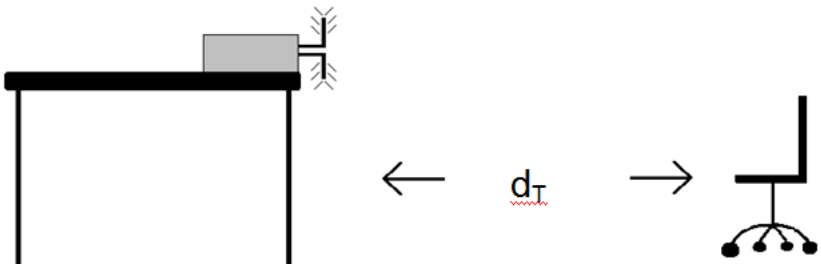

Figure 2.1: Target at distance d_T from UWB device

We aim to detect vital signs of a human-being target at a distance d_T from receiver device, ranging from 30 cm to 100 cm. Our target will be standing or sitting still at d_T distance from the radar device and breathing normally. UWB radar will be in a line-of-sight configuration with the target's chest in front and using omnidirectional antennas. Optimal condition will be no other movement in the target area (same room) during the scan, this to avoid unwanted reflection that could be hard to remove via either filtering or background noise subtraction. The scan will take no more than 1/2 minute after which data will be analyzed and elaborated by the period detection algorithm to give a best match heart and breathing rate or trigger a specific alarm as explained in Section 2.3.
We assume that the receiver device is perfectly synchronized with the transmitting

counterpart so that there is no need to handle sync issue, we also assume that the receiver can estimate and cancel any replicas referring to the static part of the channel using factory provided or built-in code.
At first we will have one or two - depending on mono or bi-static scenario - UWB radars connected directly to a personal computer running both radar control utilities and data management software. In a long term view the UWB radar could be connected to a Local Area Network, Digital Subscriber Line or even mobile phone data connection for remote monitoring and health care.

2.3.4 Background subtraction

We assume that the receiver is able to estimate and cancel all replicas referring to the static part of the channel, using background subtraction techniques [12], [13]. One problem of the measurement done is the appearance of a background signal in the captured data. This undesired signal components are caused by antenna ringing, antenna cross talk, wall reflections and non-ideal pulse generators. The main problem is that this background signal is sometimes bigger that the desired reflected pulse on the chest. On the other hand these signal components are stationary and can be subtracted from the original data. Let $v_{n,k}$ be the received sample k of scan n after some signal processing (see Chapter 4).

$$v_{n,k} = \zeta_{n,k} + c_{n,k} + \eta(n,k) \tag{2.10}$$

where $\zeta_{n,k}$ is the desired reflected pulse, $c_{n,k}$ is the stationary background and $\eta(n,k)$ is the noise. Let N be the total number of measurements, the background c_n can be estimated as

$$\hat{c}_n = \frac{1}{N}\sum_{n=1}^{N} v_{n,k} \cong c_k, \tag{2.11}$$

where $\hat{}$ denotes the estimator for c. In (2.11) all traces were averaged at the same instant k. Subtracting this estimator from the original signal leads to

$$\zeta_{n,k} \cong v_{n,k} - \hat{c}_n. \tag{2.12}$$

From (2.12) follows, that only oscillating signal components and noise remains in the signal $\zeta_{n,k}$. It is easy to understand that the stationary background will be removed at each instant sample point k. The new background reduced data can now be used as input signal.

Chapter 3

PulsOn 220 RD

3.1 Overview

The following considerations are based on a TimeDomain PulsON 220 IR-UWB device. We worked with an evaluation version of the PulsON 220 which is the natural evolution of its predecessor PulsON 210 with which shares most things. Due to the experimental nature of the Time Domain item received, it was not yet approved by FFC. We measured the PulsON 220 RD emissions also for safety. After a few tests we obtained the following data.

Pulse Repetition Frequency	9.6 MHz
Center Frequency	4.2 GHz
Bandwidth (10 dB)	2.2 GHz

Typically, UWB communications devices uses pulse with a shape that has the form of some derivative of a Gaussian pulse [14]. Time Domain, one of the pioneer manufacturers of UWB equipment and also provider of ours, declares that their PulsON technology emit ultra-short "Gaussian" monocycles. Literature knows the Gaussian monocycle as the first derivative of a Gaussian pulse. So, if a Gaussian pulse has the form $f(t) = e^{-(\frac{t}{a})^2}$ the Gaussian monocycle is

$$p(t) \propto te^{-(\frac{t}{a})^2} \tag{3.1}$$

Therefore we can approximate the transmitted signal $t(t)$ as

$$t(t) = \sum_{n=-\infty}^{+\infty} \frac{e^{-\left(\frac{(t-nT_{REP})^2}{2\sigma^2}\right)}}{\sqrt{2\pi\sigma}} \cos(2\pi f_C t + \phi_0) \tag{3.2}$$

where T_{REP} is the pulse repetition period and σ is the pulse variance. The impulse response duration is $T_P = 1000$ ps (99.91% of total energy) or $T_P = 800$ ps (99.3% of total energy) [7].

According to PulsOn notation, we define *waveform* the set of received replicas; in an ideal scenario, i.e. absence of Inter Symbol Interference (ISI) and distortion, waveform is given by the convolution of the Channel Impulse Response (CIR) and the transmitted pulse (3.2).

3.1.1 Experimental measures

The provided device is part of an educational kit by Time Domain. Due to this fact the PulsOn 220 RD received is not FCC approved. In order to measure EM field generated in our radar scenario, a fictional bistatic radar setup with both a receiver and a transmitter unit turned on was created.

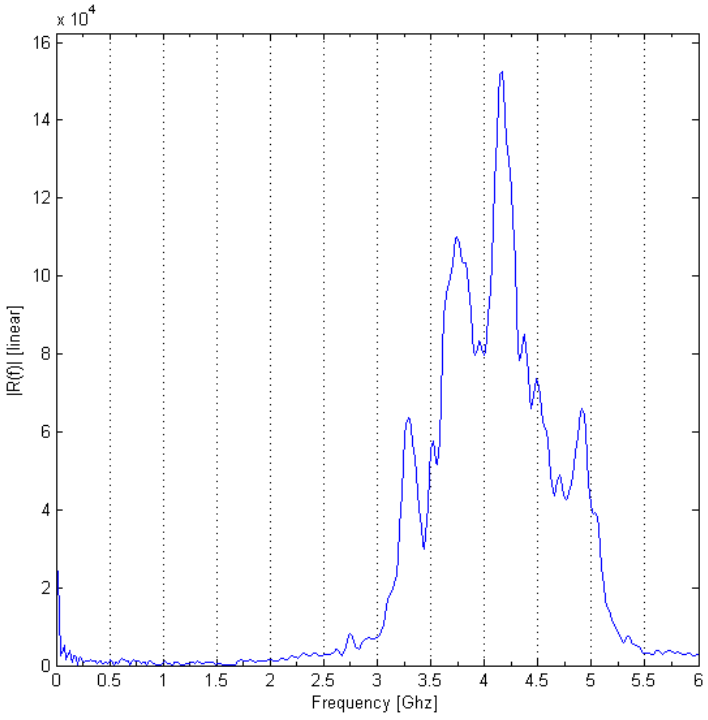

Figure 3.1: PulsON 220 RD waveform

Using a spectrum analyzer we found and confirmed 4.2 GHz as central frequency (Fig. 3.1) with a 10 dB bandwidth of 2.2 GHz, as forecasted reading PulsOn 210 RD datasheet. After trying a few different antennas the analyzer

was connected to a 32.5 dB antenna, this being the one performing best in the 3.1 ÷ 5.6 GHz range. Cables and connectors losses were ignored. It was not possible to measure EM field with the ElettroMagnetic field meter due to its maximum capable frequency of 3.0 GHz.

After few measures and scans, the antenna was moved 10 cm away from the transmitting device, this seems to be the average minimum distance between target and equipment. In this conditions the voltage value given by the spectrum analyzer was 80.50 dBμV, taking into account the 32.5 dB antenna factor we end up with a final EM value of

$$80.50\,\mathrm{dB}\mu\mathrm{V} + 32.5\,\mathrm{dB} = 113\,\mathrm{dB}\mu\mathrm{V} \tag{3.3}$$

$$113\,\mathrm{dB}\mu\mathrm{V} = 20\log(x) \tag{3.4}$$

$$x = 10^{5.65}\,\mu\mathrm{V} \tag{3.5}$$

$$x = 0.45\,\frac{\mathrm{V}}{\mathrm{m}} \tag{3.6}$$

$0.45\frac{V}{m}$.

The obtained value can be considered safe according to Italian EM field regulations. For an exposition time of more than 4 hours a day the maximum allowed EM field is 6 $\frac{V}{m}$ [15]. Italian laws concerning EM fields and emissions are one of the most restrictive among other European countries.

Table 3.1: PulsON 220 RD specs

Pulse Repetition Frequency	9.6 MHz
Center Frequency	4.2 GHz
Bandwidth (10 dB)	2.2 GHz
EM field @ 10 cm	0.45 V/m

3.1.2 PulsOn BroadSpec® P200 Antennas

Antennas for ultra wide band use must meet demanding performance specifications. They must be well-matched and efficient to take best advantage of parsimonious spectral limits. Ideally, UWB antennas should be non-dispersive or dispersive in a controlled fashion that is amenable to compensation. For a wide variety of applications, an omnidirectional response is highly desirable. Commercial operation imposes additional constraints. A mass market UWB antenna must

Table 3.2: Typical EM field

Condition	EM field $[\frac{V}{m}]$
30 m from 380.000 volt powerline	1000 ÷ 5000
Inside home	0.1 ÷ 10
Residential area	0.1 ÷ 50
30 cm from fridge	60
30 cm from blender	30
30 cm from TV	50
30 cm from electric hotplate	25
10 cm from hairdryer	100 ÷ 300
30 cm from table lamp	25

be small and inexpensive, yet must not compromise on performance. As noted in [16], the antenna accepts about 96% of applied power in band. Since the antenna is constructed on a low-loss substrate, and because resistive loading is not employed, virtually all of the accepted energy radiates. An accurate measurement of antenna efficiency across ultra-wide bandwidths poses formidable challenges, since losses in the measurement fixture tend to be much greater than losses in the antenna itself. As in [16], the provided PulsOn BroadSpec® P200 Antennas are omnidirectional and are thus well-suited for ad-hoc networks or short range detection with arbitrary azimuthal orientations. Furthermore, these antennas are electrically small and inexpensive without compromising on performance.

3.1.3 Hardware setup

The provided PulsON 220 edu kit includes 2 samples of the device and 4 antennas plus several utilities and softwares both for communication and sensing purposes. The antennas in the kit are omnidirectional so there is no specific indication on target and radar relative position. All the applications are made up of two parts: an embedded side and a host one. The embedded part runs on the device thanks to its factory provided UWB kernel, the host part runs on a Personal Computer (PC) where the software lets user choose a few settings and parameters.

Embedded and host softwares are linked together via an ethernet local area network which also includes the PC running the software. The PC sends com-

mands via network to the transmitter unit and gets data back from the receiver one, to do so it is necessary to launch two instances of the provided software.

3.1.4 Bistatic scenario

Figure 3.2: Bistatic UWB radar setup

The provided software is only capable to handle a bistatic radar setup where a unit is the transmitter and the other one is the receiver. Kernel Application Program Interface (API) helps writing from scratch a monostatic kernel side application and the software counterpart but this is out of scope. The bistatic radar mode requires an additional acquisition procedure as the transmission of a training sequence, well known at the receiver, as first step before any other data reception with the aim of defining the main communication parameters and much important to synchronize transmitter and receiver. Our bistatic scenario is made by the two units, one on top the other, with antennas as far away as possible on

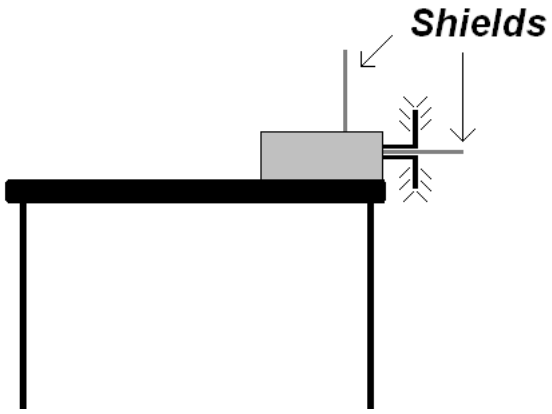

Figure 3.3: Aluminium foil shields located behind and between UWB radar devices

the same vertical line as in Fig. 3.2. For the sake of the experiments just behind the unit (opposite to antennas) there is an aluminium foil shield as in Fig. 3.3. In this way most of the "back" reflections are taken away or heavily attenuated. Just after running a few scans an other aluminium foil is put in between units to prevent direct signal from masking other reflections.
Other tests are done trying to make directional the two omnidirectional provided antennas aiming to solve the out-of-sync issue that will be discusses later on in Section 3.2.2.

3.1.5 Parameter description

To better understand the output given by the receiver software we must describe most of involved parameters.

Definition 3.1. *Pulse Repetition Frequency - RPF*

The pulse repetition frequency (RPF) is user selectable; in our scenario it has always been set to 9.6 MHz. Therefore, the symbol period $T_S = 1/RPF = 1\mu$s

Definition 3.2. *Hardware Integration - HWI*

The hardware integration (HWI) is the number of pulses integrated to build a symbol: in our scenario it has been set to 32.

Definition 3.3. *Software Integration - SWI*

The software integration (SWI) is the number of samples averaged at each step to form a single sample value. At each scan step SWI samples are summed to yield the current sample value: in our scenario it has been set to 1.

Definition 3.4. *Pulse per sample - PPS*

Pulse per sample (PPS) is the number of radio pulses required for each scan sample: PPS = HWI · SWI. In our scenario it was 32.

Definition 3.5. *Scan windowing start position - STA*

This is the start position of the scan windowing, evaluated in bins.

Definition 3.6. *Scan windowing stop position - STO*

This is the stop position of the scan windowing, evaluated in bins.

Definition 3.7. *Scan window - SW*

It is $SW = STO - STA$ measured in bins. In our scenario it was 640 bins equal to 20.34 ns.

Definition 3.8. *Step size - STEP*

The step size (STEP), given in bins, also known as waveform resolution, is the time between two successive samples. In our scenario it was 1 bin equal to 31.79 ps.

Definition 3.9. *Samples per scan - SPC*

The number of samples in a scan (SPC) is given by $SPC = \frac{SW}{STEP}$. In our scenario it was 640.

Definition 3.10. *Pulse per waveform - PPW*

The number of pulse per waveform (PPW) is the number of pulses required to build the entire waveform.

$$PPW = PPS * SPC = HWI \cdot SWI \cdot \frac{SW}{STEP}.$$

3.2 Software management

3.2.1 Bistatic radar application

To manage a bistatic radar setup we need two separate instances of BSRA, one for each side of the communication. The application let the user select a few parameters such as start and stop position, software integration and step size. Once setup is complete it is possible to start transmission and therefore the receiver module shows up. Scans are visible in realtime and can also be saved on text file for later analysis. In Fig. 3.4 we have the BSR application Setup tab, the

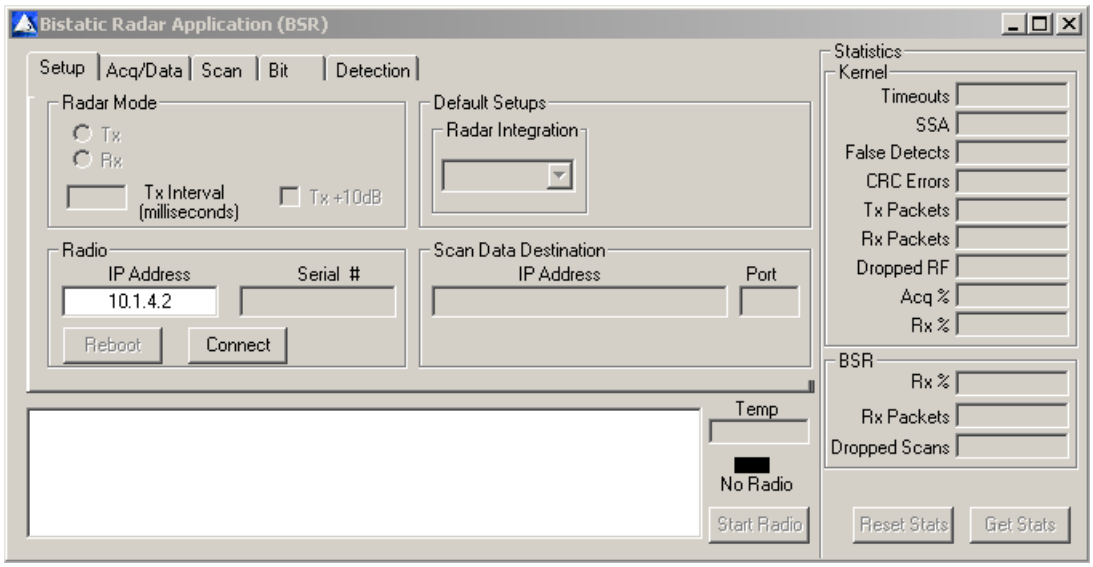

Figure 3.4: BSR application setup tab

one used to connect to the radio, set the radio mode (tx o rx), set the transmit interval (tx only) and to change radar integration. Through the interface, the user can select the desired interval between transmitted packets changing *Tx Interval* value in milliseconds. Radar integration parameter refers to the value used by the receiver integrator as later shown in Fig. 4.1; the optional field *Scan Data Destination* sets the specified IP address as destination for received scans. Bistatic Radar Application lets user control some scan parameters settings such those referring to the waveform, including the start and stop position of the scan window relative to lock spot, bit integration and step size. Fig. 3.5 shows the Scan Tab / Waveform Subtab where user can modify default *Start Pos* and *Stop Pos* values to change the starting/stopping position for the waveform scan in terms of

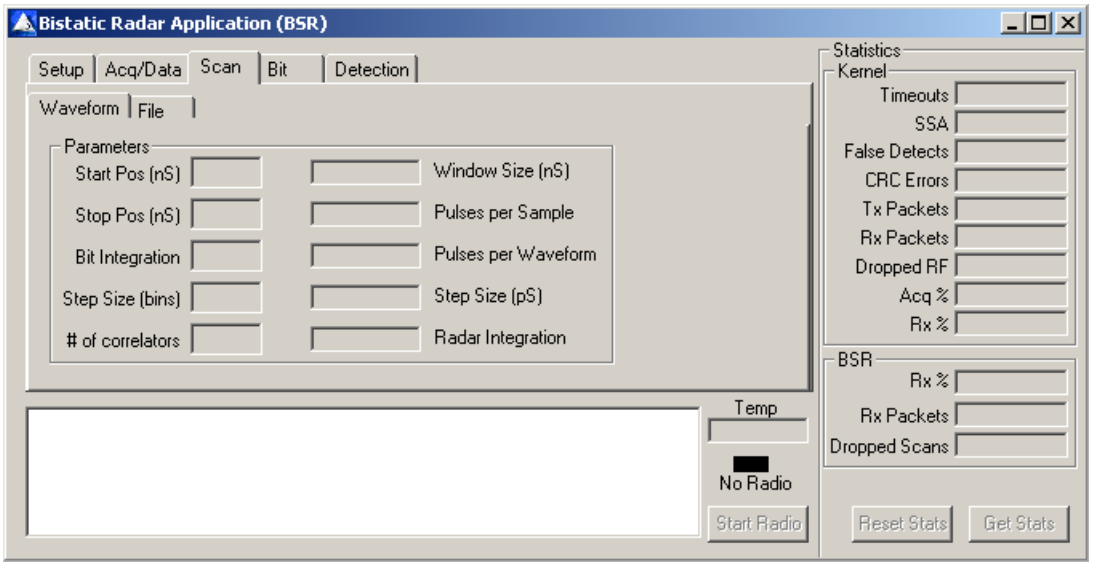

Figure 3.5: BSR application scan tab

nanoseconds offset from lockspot. Value from $-100ns$ to $100ns$ may be entered: a negative value indicates a time earlier than the lockspot and positive value indicates a time later than the lockspot. At the time radio is started, the window size is computed from the actual values calculated by the radio and displayed in the *Windows Size* field. The *Bit Integration* field specifies the number of data symbols (bits) used to generate a single point in the waveform scan. Each symbol is generated by integrating the number of pulse specified in the *Radar Integration* field seen in Fig. 3.4 and displayed in the *Pulse per Sample* field when the radio is started. To specify the time interval, measured in bins, between successive pulse sample the user can change the *Step Size* field. The minimum value accepted is 1 bin, values in bins are then shown in pS in the *Step Size (pS)* field. The conversion rule from bin to pS is $1bin = 31.789pS$.

The outputted txt file contains SPC values plus an header containing a brief summary of the setup parameters. With some Matlab scripting we are able to import the txt file, split header and data and then create an array s for the SPC values, so for each scan we have an array. In other words for N scans we build up a NxSPC matrix S [17]. We decided to group all the scans in a unique S matrix mainly to simplify successive elaborations. Each row of the S matrix is a scan, so the whole matrix contains N scans. The $i-th$ row of S, the $i-th$ scan, is

$$s_i = [v_{i,1}, v_{i,2}, ..., v_{i,SPC}] \tag{3.7}$$

where $v_{i,j}$ is the $j-th$ value of the $i-th$ scan.

$$S = \begin{bmatrix} s_1 \\ s_2 \\ \dots \\ s_N \end{bmatrix} = \begin{bmatrix} v_{1,1} & v_{1,2} & \dots & v_{1,SPC} \\ v_{2,1} & v_{2,2} & \dots & v_{2,SPC} \\ \dots & \dots & \dots & \dots \\ v_{N,1} & v_{N,2} & \dots & v_{N,SPC} \end{bmatrix} \tag{3.8}$$

No option nor parameter is provided for time synchronization and this could lead to a sync problem between successive scans.

3.2.2 Out of sync scans

The PulsON 220 units provided are factory setup for a bistatic radar scenario. In this setup we encountered a big challenge about synchronization. In the BSR application there is not setup option for sync so it might be thought that it is a kind of automatic routine at startup. Even taking a deeper look at BSR application source code is unsuccessful, it is now realistic that the sync process is done by the unit kernel without any external possible option.
Since the first scan, the BSR application shows continuous scan flow affected by a random offset that moves back and forth the waveform. Unfortunately this problem is also present in the scan text save. There is no periodicity in the offset value.
A MATLAB script is made to cope with the out-of-sync scan. The first script version, called *resync*, relies on the assumption that the maximum signal value should be at time zero so it searches the given scan for the max value and then offsets the whole array by the found value.

Even if the idea is not so bad this script cannot handle the random offset given by PulsON devices mainly because it is not always truth that maximum value impulse is a time zero.
A new script, called *sync power*, tries to sync the scans given a reference one. It is both possible to let the script find the maximum power scan and then use it as reference or give it by hand. The *sync power* script cycles through the scans and for each one computes the signal power. In this way, if not provided by hand, the signal with max power value is considered as reference: s_{ref}. The script requires to shift forward and backward the signal so a custom build *shifta* function is coded.

Program 1 MATLAB Resync algorithm

```
function [d,i] = resync(path)

[h,d]=hdrload(path);
samples = max(size(d));
[t,i] = max(d);
i = samples/2-i; %offset traslazione
tmp = d;
if (i >= 0)
    for j=1:samples
        if (j <= i)
            d(j)=0;
        else
            d(j) = tmp(j-i);
        end
    end
else
    for j=1:samples
        if (j <= -i)
            d(j)=0;
        else
            d(j) = tmp(j+i);
        end
    end
end
```

Program 2 MATLAB Shifta function

```
function d = shifta(segnale,offset)

samples = max(size(segnale));
tmp = segnale;

if (offset >= 0)
    for j=1:samples
        if (j <= offset)
            d(j)=0;
        else
            d(j) = tmp(j-offset);
        end
    end
else
    for j=1:samples
        if (j > samples-abs(offset))
            d(j)= 0;
        else
            d(j) = tmp(j-offset);
        end
    end
end
d = d';
```

As in Program 2, for a positive *offset* value the *shifta* function shifts forward the given signal while backward for negative, padding with zero the gap, providing $s_i^{(k)}$, from $s_i = [v_{i,1}, v_{i,2}, ..., v_{i,SPC}]$ where k is the offset index ranging from -SPC to SPC, where SPC is the number of samples per scan, *sync power* calculates a Mean Square Error (MSE) value

$$MSE(i,k) = \frac{||s_i^{(k)} - s_{ref}||^2}{SPC}, \tag{3.9}$$

where $s_i^{(k)}$ and s_{ref} are vectors, i is the scan index and k is the offset index. The offset, $\hat{k} = \text{argmin}(MSE)$, that minimize MSE is then used to align that single scan. Finally a threshold is introduced in order to exclude extremely out of sync scans

$$THR = \frac{MSE}{P_{ref}}, \tag{3.10}$$

given by scan MSE over reference scan power.
This scripts run quite well while resynchronizing scans of a static (or most) scenario and target but fail when the target is moving. Neither using directional antennas nor shielding receiver from "other" reflection is of any help.

3.2.3 Algorithm performance

UWB vital analysis requires realtime data elaboration therefore the *sync_power* algorithm should take no more than a few seconds to run. What makes the difference in *sync_power* runtime is the SPC value because for an SPC offset the script makes $SPC^2 + 1$ offsets and MSE estimations. A first benchmark measures runtime - in seconds - on an average personal computer while a second one measures the number of operations required by the algorithm. Test system is an Intel Core i5 750 running 64 bit OS and MATLAB and 4 Gb of ram with a set of 112 saved ($\approx 6.5s$) scans of a test scenario. A first scan set is taken without any movement in the target area, the other one instead is taken with the target breathing normally at d_T distance. Taking into consideration that on average we have a scan every $0.3s$ that is $18scan/sec$, a runtime of $65s$ - $1170scan$ - is too long for our purposes. In Fig. 3.6 we can see that runtime is linear and proportional to the offset value.

The same proportionality is not found in the number of required operations: for a given SPC offset value the script runs $SPC \cdot SPC + 1$ offset and MSE

Program 3 MATLAB Sync_Power algorithm

```
function S = sync_power(folder, thr)
x = dir(folder);
fn = {x.name};
[fn,index] = sort_nat(fn);
x = x(index); n = size(x);
max_power = 0; max_scan = 0;
min_mse = 1000;
cnt = 1;
mse = 0;
avg_thr = 0;

for i=3:n(1,1)
    path=strcat(folder,x(i).name);
    [h,d]=hdrload(path);
    power = mean(abs(d).^2);
    if power > max_power
        max_power = power;
        max_scan = i-3;
    end
end

path=strcat(folder,x(max_scan).name);
[h,d]=hdrload(path);
max_scan_w = d;

for i=3:n(1,1)
    path=strcat(folder,x(i).name);
    [h,d]=hdrload(path);
    mse = 0;
    for j=-640:1:640
     offset_s = 641; d_tmp = shifta(d,j);
     mse(j+offset_s) = sum(abs(max_scan_w - d_tmp).^2);
     mse(j+offset_s) = mse(j+offset_s) ./ max(size(d_tmp));
    end
    [min_mse offset] = min(mse);
    d = shifta(d,offset-offset_s);
    power_t = sum(abs(d).^2);
    c_thr = min_mse ./ max_power;
    if (c_thr < thr)
        S(cnt,:) = d; cnt = cnt + 1;
    end
end
```

estimations for a total of about $5 \cdot SPC^2$ operations that is a square evolution. Each MSE estimation requires five operations: a sum, an absolute value, a square, a division and a maximum value calculation. In Fig. 3.7 we can see that required operations goes square with the offset value. Another important thing to note is that not all scans are inserted in the S matrix, *sync_power* selects scans according to the given threshold value. Threshold is the result of minimum current scan MSE over reference scan/signal power, i.e. a threshold value of 0.1 means that the current signal MSE is 10% of the reference.
According to Fig. 3.8 there is no real difference in terms of accepted scans between SPC and $SPC/2$ offset so the second one is a good choice with a runtime of about $30s$ and four times less operations to run. *Sync_power* algorithm runs quite well in the static scenario but with the target in place the random offset added by the PulsON 220 makes the synchronization much more difficult and most of the times unsuccessful. In Fig. 3.9 we see how, in a non static scenario, for a given

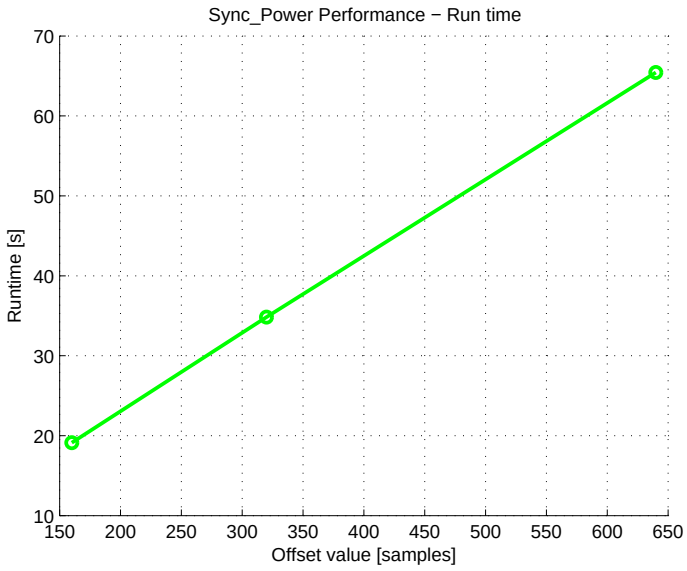

Figure 3.6: Sync_Power algorithm runtime for 112 scans

threshold level the number of accepted scans is lower than the static scenario. This not only means we have less data on which run period estimation but also we do not have any assurance on the continuity of selected scans and this may lead to impossible heart beat and breathing rate detection.

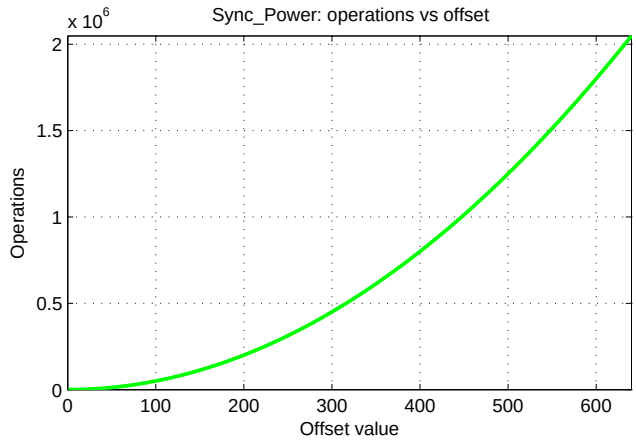

Figure 3.7: Sync_Power algorithm operation vs offset value

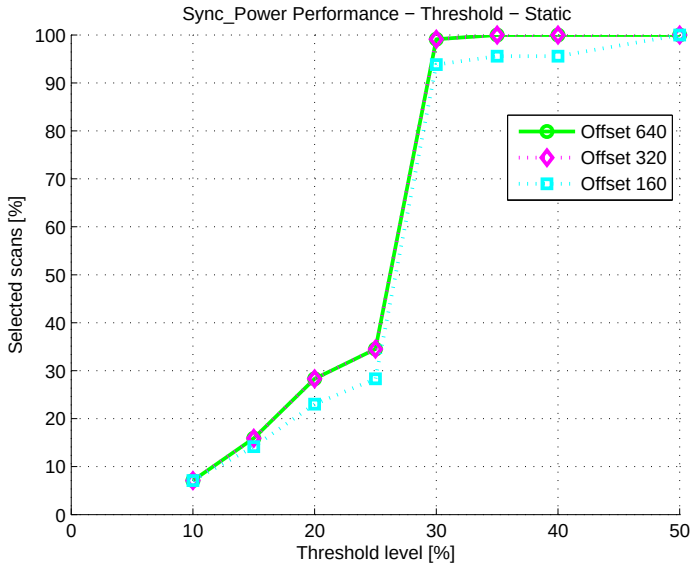

Figure 3.8: Sync_Power algorithm threshold in static scenario

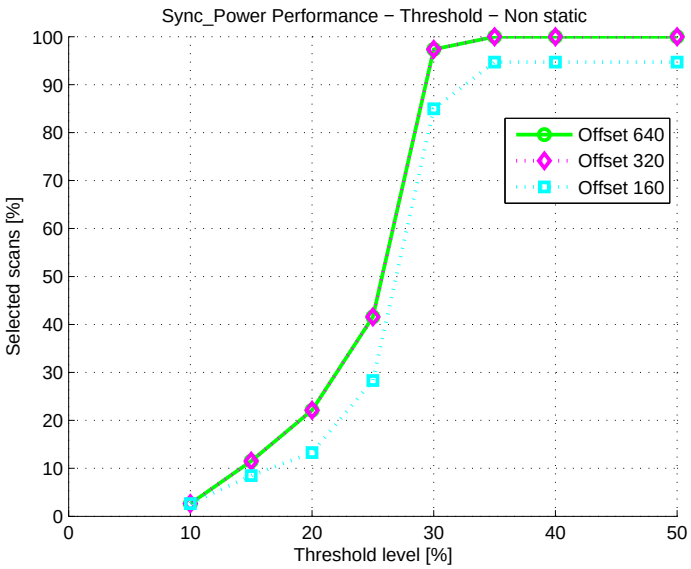

Figure 3.9: Sync_Power algorithm threshold in a non static scenario

Chapter 4

Signal processing

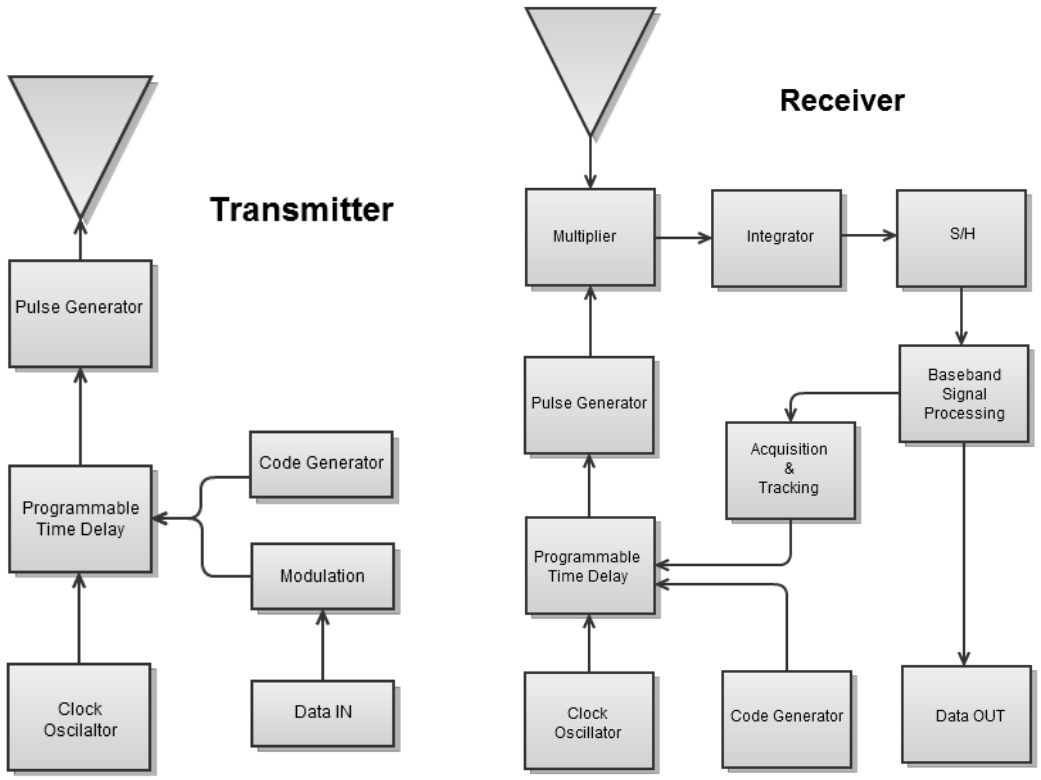

(a) Transmitter (b) Receiver

Figure 4.1: UWB Tx - Rx block diagram

4.1 Baseband operation

As we can see in Fig. 4.1, after some internal processing operations the PulsOn device outputs the received signal $v_{n,k}$ that is bandpass and both function of n, index of the current scan and k, index of current delay in the received signal of scan n, i.e.

$$v_{n,k} = \sum_{i=1}^{SPC} \gamma_i(n)\cos(2\pi f_C k + \phi_i(n))\delta(k-i) + \eta(n,k),$$

where $\eta(n,k)$ is the noise. Baseband operation is performed on the k dimension; if $f_C T_{SCAN} \in Z$, and if the low pass filter has impulse response shorter than the pulse repetition period, performing the baseband operation on each waveform scan is the same as performing it before the sampling process. In fact, if the sampling process comply the sampling theorem, it is equivalent to perform the baseband operation before or after the sampler.
As in [18], in the absence of ISI, the combination that maximizes the Signal to Noise Ratio (SNR) is given by a matched filter, i.e.

$$g_1(t) = p^*(-t + SPC/2).$$

To cope with distortion occurred during transmission due to interaction with the human body or to the presence of multiple scatterers, we consider the *estimated matched filter* and the *average filter* among the theoretical math filter.

4.1.1 Estimated matched filter

The estimated matched filter is the optimal linear filter [18] for maximizing the SNR in presence of additive stochastic noise. We assume the received baseband signal matrix S to be the result of an unknown transmitted pulse propagated in a Average White Gaussian Noise (AWGN) scenario hence all variations in the channel even those due to target vital signs are supposed like Gaussian white noise.
The estimated pulse $\hat{p}(k)$ is given by

$$\hat{p}(k) = \frac{1}{N}\sum_{j=1}^{N} v_{j,k}, \tag{4.1}$$

and the estimated matched filter $g_2(k)$ is

$$g_2(k) = \hat{p}^*(-k + SPC/2). \tag{4.2}$$

4.1.2 Average filter

The simplest solution for an average filter is the rectangular one, i.e.

$$g_3(k) = rect\left(\frac{k - SPC/2}{SPC}\right). \tag{4.3}$$

The rectangular filter combines samples by averaging them.

4.2 Period estimation

4.2.1 Welch algorithm

Welch algorithm is a method for the application of the fast Fourier transform to the estimation of power spectra, which involves sectioning the signal, taking modified periodograms of these sections, and averaging these modified periodograms. It involves the transformation of sequences which are shorter than the whole record which is an advantage when computations are to be performed on a system with limited core storage [19]. Let $X(j)$, $j = 0, ..., N-1$ be a sample from a stationary, second-order stochastic sequence. Assume for simplicity that $E(X) = 0$. Let $X(j)$ have spectral density $P(f)$,$|f| \leq \frac{1}{2}$. We take segments, possibly overlapping, of length L with the starting points of these segments D units apart. Let $X_1(j), j = 0, ..., L-1$ be the first such segment. Then

$$X_1(j) = X(j) \quad j = 0, ..., L-1. \tag{4.4}$$

Similarly,

$$X_2(j) = X(j + D) \quad j = 0, ..., L-1, \tag{4.5}$$

and finally

$$X_k(j) = X(j + (K-1)D) \quad j = 0, ..., L-1. \tag{4.6}$$

We suppose we have K such segments; $X_1(j), ..., X_k(j)$, and that they cover the entire record, i.e., that $(K-1)D + L = N$. This segment is illustrated in Fig. 4.2. The method of estimation is as follows. For each segment of length L we calculate a modified periodogram. That is, we select a data window $W(j), j =$

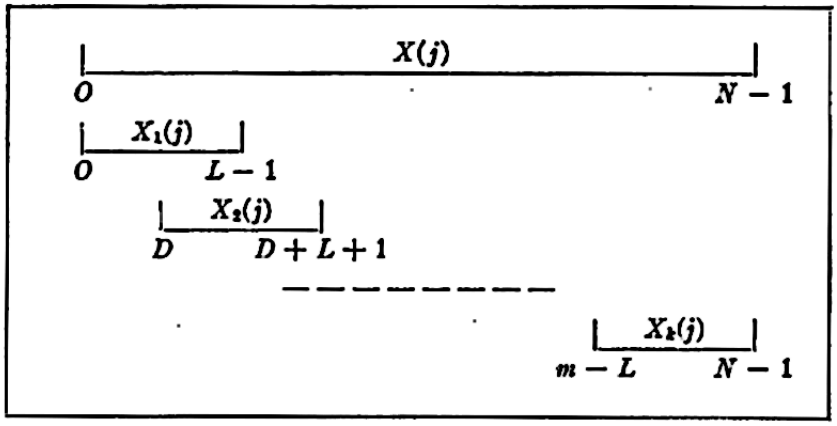

Figure 4.2: Welch record segmentation

$0, ..., L-1$ and form the sequences $X_1(j)W(j), ..., X_k(j)W(j)$. We then take the finite Fourier transform $A_1(n), ..., A_k(n)$ of these sequences. Where

$$A_k(n) = \frac{1}{L}\sum_{j=0}^{L-1} X_k(j)W(j)e^{-2kijn/L}, \tag{4.7}$$

and $i = (-1)^{1/2}$. Finally, we obtain the K modified periodograms

$$I_k(f_n) = \frac{L}{U}|A_k(n)|^2 \quad k = 1, 2, ..., K, \tag{4.8}$$

where

$$f_n = \frac{n}{L} \quad n = 0, ..., L/2, \tag{4.9}$$

and

$$U = \frac{1}{L}\sum_{j=0}^{L-1} W^2(j). \tag{4.10}$$

The spectral estimate is the average of these periodograms, i.e.,

$$\hat{P}(f_n) = \frac{1}{K}\sum_{k=1}^{K} I_k(f_n). \tag{4.11}$$

Now we can show that

$$E[\hat{P}(f_n)] = \int_{-1/2}^{1/2} q(f)P(f - f_n)df, \tag{4.12}$$

where

$$q(f) = \frac{1}{LU} \left| \sum_{j=0}^{L-1} W(j) e^{2\pi i f j} \right|^2 , \tag{4.13}$$

and

$$\int_{-1/2}^{1/2} q(f) df = 1. \tag{4.14}$$

Hence, we have a spectral estimator $\hat{P}(f)$ with a resultant spectral window whose area is unity and whose width is of the order of $1/L$. The WELCH estimator is

$$P_{WELCH} = \frac{1}{K} \sum_{k=1}^{K} I_k(f_n), \tag{4.15}$$

where K is the number of segments. We apply the Welch algorithm at each scan, i.e.

$$X(j) = v_{n,j}. \tag{4.16}$$

4.2.2 MUSIC algorithm

The term MUltiple SIgnal Classification (MUSIC) describes experimental and theoretical techniques involved in determining the parameters of multiple wavefronts arriving at an antenna array from measurements made on the signals received at the array elements. MUSIC algorithm can provide estimates of: number of signals, direction of arrival, strengths and cross correlation among the directional waveforms, polarizations and strength of noise. Applications are: conventional interferometry, monopulse direction finding and multiple frequency estimation [20].

MUSIC estimates the frequency content of a signal or autocorrelation matrix using an eigenspace method. This method assumes that a signal, $G(n)$, consists of w complex exponentials in the presence of Gaussian white noise. Given an MxM autocorrelation matrix, R_x, if the eigenvalues are sorted in decreasing order, the eigenvectors corresponding to the w largest eigenvalues span the signal subspace. Note that for $M = W + 1$, MUSIC is identical to Pisarenko's method [21]. The general idea is to use averaging to improve the performance of the Pisarenko estimator.

4.2.3 AMDF technique

Average Magnitude Difference Function is a variation on autocorrelation analysis where, instead of correlating the input signal at various delays (where multiplications and summations are performed at each value of delay), a difference signal is made between the delayed signal and the original and, at each delay, the absolute magnitude of the difference is taken. The difference signal is always zero at delay, and exhibits deep nulls at delays corresponding to the pitch period. Some of the reasons the AMDF is attractive include the following: it is a simple measurement which gives a good estimate of pitch contour, it has no multiply operations, its dynamic range characteristics are suitable for implementation on a 16-bit machine and the nature of its operations makes it suitable for implementation on a programmable processor or in a special purpose hardware [22]. It is well known that the autocorrelation function (ACF) of a signal signal (of suitable length) can be used for pitch detection [22]. A variation of autocorrelation analysis for measuring the periodicity of signal uses the AMDF, defined by the relation

$$D_\tau = \frac{1}{L}\sum_{j=1}^{L} |X(j) - X(j-\tau)|\,, \quad \tau = 0, 1, ..., \tau_{max}, \tag{4.17}$$

where $X(j) = v_{n,j}$ are the samples of input signal and $X(j-\tau)$ are the sample time shifted by τ seconds. The vertical bars denote taking the magnitude of the difference $X(j) - X(j-\tau)$. Thus a difference signal D_τ is formed by delaying waveform from the original, and summing the magnitude of the differences between sample values. An approximate expression that provides a useful relationship between the AMDF and the ACF os a sampled sequence will now be developed. This relationship is based on the well known bound,

$$\frac{1}{K}\sum_{k=1}^{K} |X(k)| \leq \left(\frac{1}{K}\sum_{k=1}^{K} X(k)^2\right)^{\frac{1}{2}}. \tag{4.18}$$

In (4.18), the left side is the average magnitude of the samples sequence $X(k)$ while the right side of the equation is the root mean square (RMS) value of the sequence. The AMDF for a sequence of sample $X(k)$ is defined by the relation

$$D_n = \frac{1}{K}\sum_{k=1}^{K} |X(k) - X(k-n)|, \tag{4.19}$$

where the delay index n ranges from $-(N-1)$ to $(N-1)$. In implementing (4.19), the summing index k ranges from $k = n$ to $k = N-1$ for $n \geq 0$. That

is, the AMDF is formed only in the region of overlap of the sequences $X(k)$ and $X(k-n)$. Thus for $n < 0$, the summing index k ranges from 0 to $N - 1 + n$. It is seen that D_n is an even function (i.e., $D_n = D_{-n}$) according to the above definitions. Using (4.18) we can approximate D_n in the form

$$D_n = \frac{1}{K}\sum_k |X(k) - X(k-n)| = \kappa_n \left(\frac{1}{K}\sum_k (X(k) - X(k-n))^2\right)^{\frac{1}{2}}. \quad (4.20)$$

In (4.20), the coefficient κ_n is a scale factor. For Gaussian sequences it is possible to determine a value for κ_n (analytically) that would achieve equality on the average between the average magnitude and rms sums. For other distributions, a value for κ_n can be determined experimentally by testing a large number of sequences. It is evident that κ_n depends upon the joint probability density function (PDF) of $X(k)$ and $X(k-n)$. Since the join pdf of $X(k)$ and $X(k-n)$ will in general vary with the delay index n, the coefficient κ_n will therefore be a function of n. By expanding the squared term in braces under the square root sign in (4.20) we can express D_n in the form,

$$D_n = \kappa_n \left(\frac{1}{K}\sum_k X(k)^2 + \frac{1}{K}\sum_k X(k-n)^2 - \frac{2}{K}\sum_k X(k)X(k-n)\right)^{\frac{1}{2}}. \quad (4.21)$$

Defining the ACF of the sequence $X(k)$ as

$$R_n = \frac{1}{K}\sum_k X(k)X(k-n), \quad (4.22)$$

it is seen that the third sum in the braces is $-2R_n$. Assuming that the sequence $X(k)$ corresponds to a stationary process it is evident that the first two sums in (4.21) are simply the ACF evaluated at $n = 0$. That is

$$R_0 = \frac{1}{K}\sum_k X(k)^2 = \frac{1}{K}\sum_k X(k-n)^2, \quad (4.23)$$

under the assumption of stationarity. Using (4.22) and (4.23) in (4.21) yields D_n as

$$D_n = \kappa_n [2(R_0 - R_n]^{\frac{1}{2}}. \quad (4.24)$$

The properties of the AMDF are accurately characterized by (4.24). Specifically, the AMDF is seen to be zero adat zero delay ($n = 0$) and varies as the square

root of the ACF that has been negated and inversely shifted by R_0. Nulls will appear in D_n at those points where R_n is large compared with R_0. This occurs when the sequence $X(k)$ is taken from a signal sound containing two or more pitch periods in the sequence. The separation of the nulls is a direct measure of the pitch period. The AMDF estimator is [23]

$$P_{AMDF} = \text{argmin}_{\phi=\phi_{min}}^{\phi_{max}}(D_\phi) \tag{4.25}$$

where ϕ_{min} and ϕ_{max} are respectively the possible maximum and minimum period value.

4.2.4 ML algorithm

Maximum Likelihood (ML) algorithm is a new technique to estimate unknown period of signal within a range when the signal is zero mean and unknown shape. The technique is particularly effective when the tested signal has strong periodic components outside the considered range, e.g. as a consequence of the superposition of signals with periods in different ranges. The proposed method provides the ML estimate in case the signal is periodic and affected by Gaussian noise [24]. We aim to estimate the period of the signal starting from the noisy observation of K samples

$$v_{n,k} = \zeta_{n,k} + \eta(n,k) \tag{4.26}$$

where $k = 1, ..., K$ and $\eta(n,k)$ is an Independent and Identically Distributed, zero mean white process with power σ_η^2. The choice of observed samples K is subjected to the fact that the signal $\zeta_{n,k}$ may be regarded as periodic only for a limited time and with unknown period. This is the case of vital signs which can be assumed periodic as long as the target conditions do not change. We assume that the period is limited to a range of M values in the set I_P. We aim at evaluating the likelihood that the signal $\zeta_{n,k}$ has period P and we evaluate the vector obtained by averaging the observed samples over

$$L_P = \left\lceil \frac{K}{P} \right\rceil \tag{4.27}$$

candidate period sample. In particular, let

$$\mu_n = [v_{n,0}, v_{n,1}, ..., v_{n,L_P-1}]. \tag{4.28}$$

Then the average over L_P samples is

$$m_P(n,k) = \frac{1}{L_P}\sum_{l=0}^{L_P-1} v_{n,k+lP} \tag{4.29}$$

$$= \frac{1}{L_P}\sum_{l=0}^{L_P-1} \zeta_{n,k+lP} + \hat{\eta}_P(n,k) \tag{4.30}$$

$$k = 0, 1, ..., P-1, \tag{4.31}$$

where

$$\hat{\eta}_P(n,k) = \frac{1}{L_P}\sum_{l=0}^{L_P-1} \eta(n,k+lP) \tag{4.32}$$

with power σ_η^2/L_P. The proposed technique is based on the idea that multiple signal periods will sum up coherently. From now, $rep_{L_P}m_P$ is the vector of periodic repetition of $m_P(n,k)$ performed L_P times; this vector is so length L_PP. In case of P equal to period of observed signal $\hat{P}$, as $K \to \infty$ we have $rep_{L_P}m_P(n,k) \to \zeta_{n,k}$. So the $rep_{L_P}m_P(n,k)$ is an estimate of $\zeta_{n,k}$ and we can now apply ML estimation on $\zeta_{n,k}$ under assumption that the period of $\zeta_{n,k}$ is P.
Let $f(\mu_n|P)$ be the conditional probability density function (PDF) of μ_n given that $\hat{P} = P$. The log-likelihood function is

$$\Lambda_P = \log f(\mu_n|P) \tag{4.33}$$

and the ML estimator is

$$P_{ML} = \text{argmax}_{P\in I_P}\Lambda_P \tag{4.34}$$

where the maximization can be found by an exhaustive search over the possible candidate period set I_P. Taking into account that the conditional PDF of a zero mean Gaussian vector μ_n [24] is

$$f(\mu_n|P) = \frac{1}{(2\pi)^{N/2}\left(\frac{P\sigma^2}{L_P}\right)^{1/2}} e^{-(1/2)(L_P/\sigma^2)||\mu_n - rep_{L_P}m_P||^2} \tag{4.35}$$

the log-likelihood function for a candidate period P is

$$\Lambda_{n,P} = -\log\left[(2\pi)^{N/2}\left(\frac{P\sigma^2}{L_P}\right)^{1/2}\right] - \frac{1}{2}||\mu_n - rep_{L_P}m_P||^2. \tag{4.36}$$

4.2.5 Low Complexity ML estimation

In [24], it is proposed a low complexity (LC) approximation of the ML estimate. Consider the estimate correlation

$$C(n,p) = \frac{1}{K}\sum_{k=1}^{K} v_{n,k}(v^*_{n,k+p})_K, p = 1, ..., K \tag{4.37}$$

where $(a)_K = a \bmod K$. If the signal has period P and zero mean, the average autocorrelation function

$$\frac{1}{L_P}\sum_{m=0}^{L_P-1} C(n, mP), \tag{4.38}$$

is periodic with the same period of the signals. In details, if $v_{n,k}$ includes a large number of periods, i.e., $L_P \gg \sigma^2_\eta$ we have

$$\frac{1}{L_P}\sum_{m=0}^{L_P-1} C(n, mP) = \frac{1}{P}\sum_{l=0}^{P-1}\frac{1}{L_P^2}\sum_{i=0}^{L_P-1}\sum_{j=0}^{L_P-1} v_{n,l+iP}v^*_{n,l+jP} \tag{4.39}$$

$$= \frac{1}{P}\sum_{l=0}^{P-1}|\delta(l,P)|^2, P \in I_P \tag{4.40}$$

where

$$\delta(l,P) = \frac{1}{L_P}\sum_{m=0}^{L_P-1} v_{n,l+mP}, l = 0, 1, ..., P-1. \tag{4.41}$$

The idea behind this new method is that the sum in (4.41) allows the averaging of the noise and so a reduce noise impact on the final estimate. The average autocorrelation can be computed with a reduced complexity with respect to (4.37), by first computing $\delta(l,P)$ and then using (4.40). Assuming $L_P P \approx N$ the LC method can be written as

$$P_{LC} = \text{argmax}_{P\in I_P}\frac{1}{2\sigma^2_\eta P}\sum_{l=0}^{P-1}|\delta(l,P)|^2. \tag{4.42}$$

The average autocorrelation is affected by a noise componenet with mean σ^2_η/L_P. If an estimate of the noise power is available, we can further refine the LC method by removing the mean value of the noise component, obtaining the LC2 method

$$P_{LC2} = \text{argmax}_{P\in I_P}\frac{1}{2\sigma^2_\eta P}\sum_{l=0}^{P-1}|\delta(l,P)|^2 - \frac{\sigma^2_\eta}{L_P}. \tag{4.43}$$

4.2.6 Weight algorithm

An different autocorrelation based algorithm is presented in [25]. The WEIGHT method uses an autocorrelation function weighted by the inverse of an AMDF. The AMDF produces a notch, while the autocorrelation function does a peak. The idea behind this method is that because the autocorrelation function and AMDF have independent statistics each other, the peak of the autocorrelation function may be emphasized if the autocorrelation function is combined with the inversed AMDF. If the true peak corresponding to the pitch period is emphasized, it is expected that the resulting accuracy of pitch extraction for the weight is improved. The autocorrelation function $\psi(\tau)$ is calculated by

$$\psi(\tau) = \frac{1}{N}\sum_{n=0}^{N-1} v_{n,k} v^*_{n,k+\tau}, \tag{4.44}$$

where $v_{n,k}$ is the input signal and τ the delay. The characteristic of $\psi(\tau)$ is that it has a large value when $v_{n,k}$ is similar with $v_{n,k+\tau}$. If $v_{n,k}$ has a period P, then $\psi(\tau)$ has peaks at $\tau = lP$ where l is an integer.
Essentially, $\psi(0)$ gives the largest value among $\psi(\tau)$ with $\tau = lP$. The second value is given by $\psi(P)$. Other peaks of $\psi(\tau)$ decrease as τ increases. Therefore, we can estimate the pitch period P from the location of the peak at $\tau = P$. We have an autocorrelation function given by

$$\psi(\tau) = \frac{1}{N}\sum_{n=0}^{N-1}(\zeta_{n,k} + \eta(n,k))(\zeta_{n,k+\tau} + \eta(n,k+\tau) \tag{4.45}$$

$$= \psi_1(\tau) + 2\psi_2(\tau) + \psi_3(\tau) \tag{4.46}$$

where $\psi_1(\tau)$ is an autocorrelation function of $\zeta_{n,k}$, $\psi_2(\tau)$ is a cross-correlation function of $\zeta_{n,k}$ and $\eta(n,k)$ and $\psi_3(\tau)$ is an autocorrelation function of $\eta(n,k)$. If $\zeta_{n,k}$ does not relate with $\eta(n,k)$, then $\psi_2(\tau) = 0$. Furthermore, if $\eta(n,k)$ is uncorrelated, then $\psi_3(\tau) = 0$ except for $\tau = 0$. In such a case,

$$\psi_1(\tau) = \psi_1(\tau) + \psi_3(\tau), \tau = 0 \tag{4.47}$$

$$\psi_1(\tau) = \psi_1(\tau), \tau \neg 0 \tag{4.48}$$

are both valid. Based on these properties, the WEIGHT provides robust performance against noise. The autocorrelation function with period P has some peaks at the locations of lP. Although the maximum peak is located at $\tau = P$ except

for the case of $\tau = 0$, in some cases, the peak located at $\tau = 2P$ becomes larger that that located at $\tau = P$. For the purpose of emphasizing the true peak for the WEIGHT, [25] proposes an autocorrelation function weighted by an inversed AMDF. The AMDF is described by (4.19). The proposed function is then given by

$$f(\tau) = \frac{\psi(\tau)}{D_\tau + \varphi}, \tag{4.49}$$

where $\varphi > 0$ is a fixed number. The difference function in (4.19) provides at $\tau = 0$

$$D_0 = 0. \tag{4.50}$$

Therefore,

$$\frac{1}{D_0} = \infty. \tag{4.51}$$

For this reason the denominator in (4.49) is stabilized by adding φ. Finally, the WEIGHT estimator is

$$P_{WEIGHT} = \text{argmin}_{P \in I_P} f(P). \tag{4.52}$$

4.2.7 CORR algorithm

The CORR algorithm is the simplest among the period detection algorithms presented. It is based on the autocorrelation function $C(n, p)$ and provides

$$P_{CORR} = \text{argmax}_{P \in I_P} C(n, p) \tag{4.53}$$

4.2.8 Comparison

The matched filter output is an unknown periodic signal result of breathing and heart beat signals sum. In a healthy adult both breathing and heart rate are periodic. The average respiratory rate is usually given as 12 breaths per minute [26] - i.e. $\frac{12}{60}Hz = 0.2Hz$ with a at rest range of $12-20$ breaths per minute; typical healthy resting rate in adults is $60-80$ beats per minute [26] - ie. $\frac{70}{60}Hz = 1.16Hz$. Period estimation for UWB vital signs monitoring is required to be in realtime or with a very short delay otherwise it is useless. Period estimators algorithm are divided in two classes. The first one is based on the signal correlation, either

in time domain, [27] [28] [29], or with the support of a Fourier analysis. The other class is based on the notion that the difference of two signal period is zero, AMDF [30]. Widely used algorithms for peak detection are Welch and PMUSIC algorithm. A new technique to estimate unknown period of a signal within a range is proposed in [24]. This technique is particularly effective when the tested signal has strong periodic components outside the considered range. The method provides the ML estimate in case the signal is periodic and affected by Gaussian noise. The ML estimator applied in the estimation of heart rate from a UWB radar signal outperform the state of art methods even in a short observation of the periodic signal [24].
To compare the estimation methods we evaluate the normalized (respect to the period) MSE defined as (in dB)

$$\rho = 10\log_{10}\{E[|\bar{P} - P_{est}|]/\bar{P}\}, \tag{4.54}$$

where P_{est} is the period estimate, $\bar{P}$ is the target known heart rate and the power is normalized with respect to the period. Figure 4.3 is the result of period

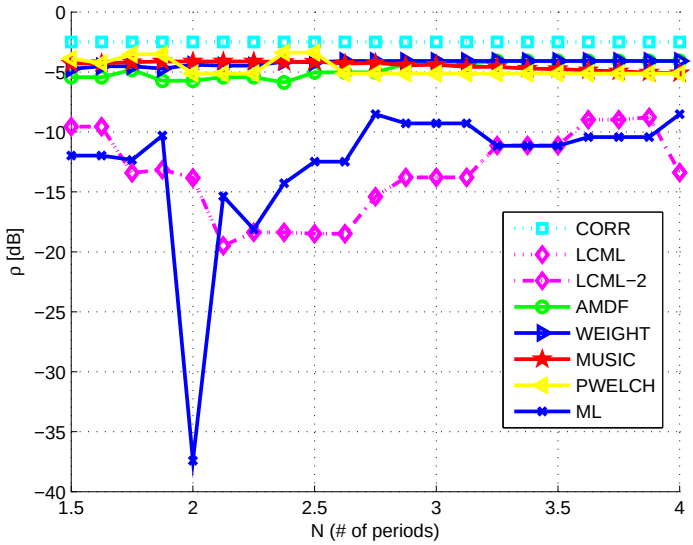

Figure 4.3: Normalized MSE of the estimated heart beat period as a function of N/P. Experimental result. No filter applied.

estimation comparison run on real data taken in lab, as it can be clearly seen ML and LCML are the two algorithms that performs best.

4.2.9 Filter improvement

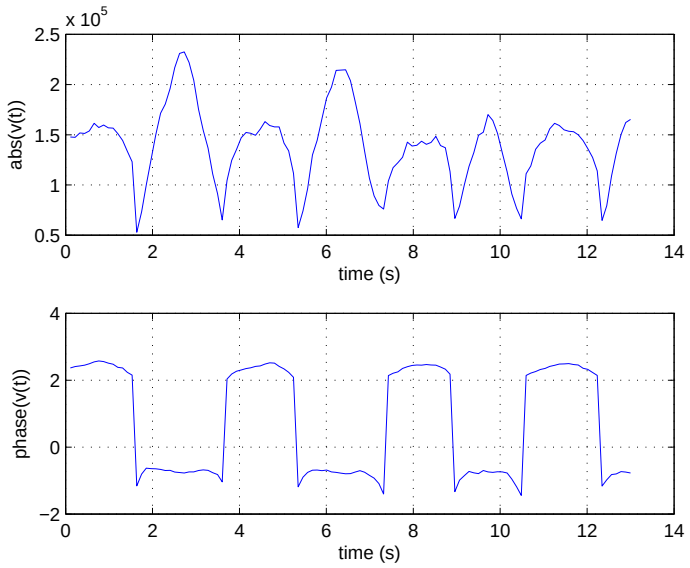

Figure 4.4: Breating and heart beat signal

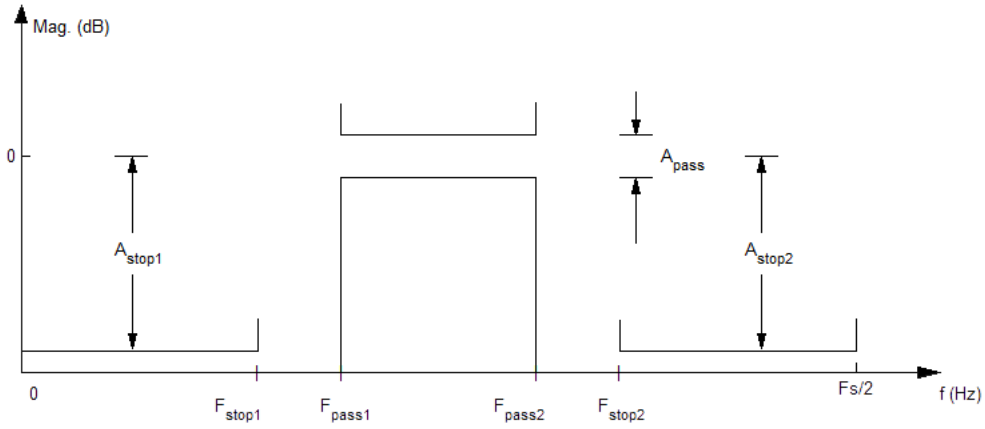

Figure 4.5: Passband filter design schema

The signal s_k is the sum of both heart and breath rate, Fig. 4.4 represent the absolute and phase value of s_k. To achieve our object and get a final heart beat rate indication we need to filter out the unwanted breath depending periodic component. A filter is developed to highlight the heart beating component against breathing. The idea is to remove the frequency components out of potential heart rate range that is, for a healthy man, $60 - 90$ beat per minute (BPM). To widen

the selection we consider rates in range $50 - 120$ bpm that in terms of frequency corresponds to $0.8Hz - 2Hz$. We aim to remove frequency components outside *0.8 Hz* and *2 Hz* with a low ripple in both pass and stop band to reduce the chance of altering original signal.

Program 4 MATLAB filter design

```
Fs = 9.1553;
f0 = 0.71;
f1 = 0.99;
f2 = 2.0;
f3 = 2.28;
f = [0 f0 f1 f2 f3 Fs./2];
f = f ./ (Fs./2);
a = [0 0 10 10 0 0];
n = 40; %requested filter order

b = firpm(n,f,a);
```

Table 4.1: Optimal filter requirements

Parameter	Value
F_s	9.1553
F_{stop1}	0.71 Hz
F_{pass1}	0.99 Hz
F_{pass2}	2 Hz
F_{stop2}	2.28 Hz
A_{stop1}	10^{-3}
A_{pass}	10^{-1}
A_{stop2}	10^{-3}

We also at finding a best performing filter with the minimum order, so the transient requires as minimum samples as possible. We use requirements in Tab. 4.1 to run the filter order comparison. The filter order comparison is focused on 2.5 and 3 periods that correspond to about 74 and about 89 samples and seems a right choice even for long transient filters. Fig. 4.6 and 4.7 show the various

period detection algorithms ρ values compared against filter length. In Fig. 4.6

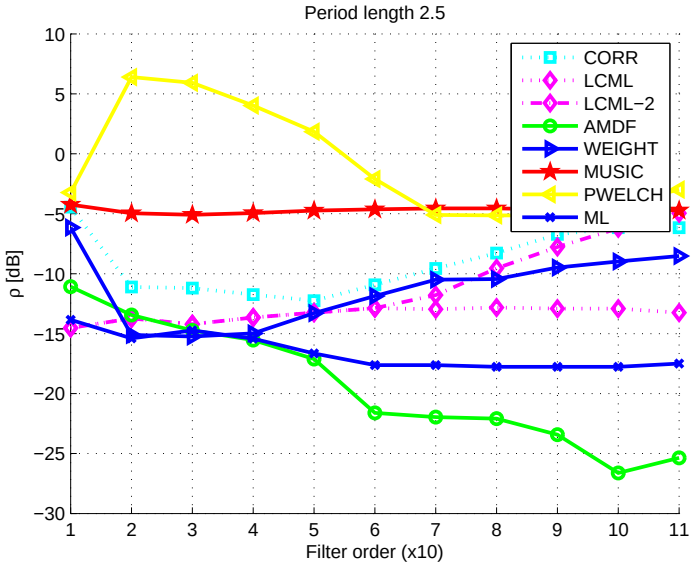

Figure 4.6: Period 2.5 filter order comparison

we clearly see that for a filter order greater than 20 the AMDF technique performs very well with more than $15dB$ improvement and also the ML gains about $5dB$ starting from the same order. Also CORR and WEIGHT gain a few dB but only for filter order in range $20-50$. Other algorithms do not show any benefit - around 2.5 period - from the application of any order filter.
In Fig. 4.7 we see the ML does not gain any dB while WEIGHT gains $\approx 11dB$ for filter order in range $20-40$, AMDF gains more or less the same as WEIGHT but in $60-80$ range and finally CORR gains $\approx 10dB$ in $20-40$ range. Remaining algorithms underperforms in the whole filter order range.
In Fig. 4.8 we see general improvement except for MUSIC and PWELCH. ML gains $\approx 7dB$ from order 60, LCML gains as ML but limited to $60-70$ order. AMDF gains $\approx 8dB$ from order 20, WEIGHT gains $\approx 10dB$ in $20-40$ filter order range. Finally CORR performs $\approx 12dB$ better in order range $20-40$.

As a result of the previous comparison we decide to design two filters: one with order 30 and the other with order 70 in order to enhance performance of WEIGHT, AMDF and CORR algorithms. The first filter should enhance best WEIGHT and CORR while the second should do the same for AMDF, LCML and ML.
Fig. 4.9 is the 30-th order filter response and Fig. 4.10 is the 70-th order filter

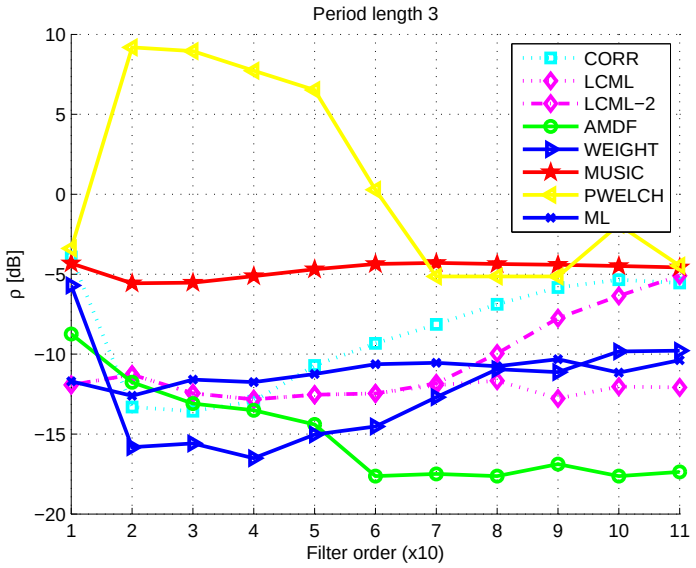

Figure 4.7: Period 3 filter order comparison

response.

The difference equation that defines the output of a FIR filter in terms of its input is:

$$y[n] = b_0 v_{i,n} + b_1 v_{i,n-1} + ... + b_N v_{i,n-N} \tag{4.55}$$

where $y[n]$ is the $n-th$ filtered scan and b_i are the filter coefficients also known as tap weights and N is the filter order. A Nth-order filter has $(N+1)$ terms on the right-hand side that are commonly referred to as taps. The filter equation can also be expressed as a convolution of the coefficient sequence b_i with the input signal:

$$y[n] = \sum_{i=0}^{N} b_i s_{n-i} \tag{4.56}$$

As we can see in Fig. 4.11 the 30-th order filter reduces the average ρ value, particularly for WEIGHT, CORR and in general we see improvements to all algorithms except for PWELCH algorithm which underperforms. In Fig. 4.12, the 70-th order filter MSE, we see the improvements to LC and LCML as wanted. There is no great difference in AMDF performance with 30-th or 70-th order filter.

Using a filter between mixed breathing and heart rate signal and period estimator seems a good choice to achieve a lower ρ value that is a more precise P_{est} period estimation. The idea to design two filters for difference period detection algorithm performance achievement does not give the expected improvement re-

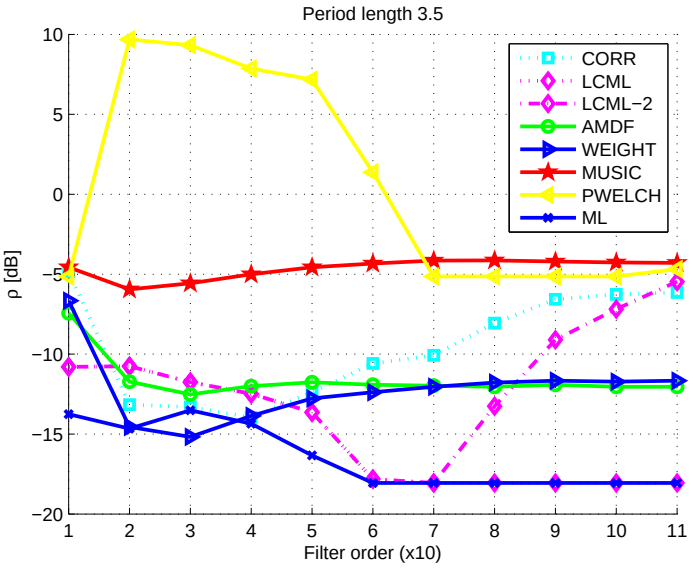

Figure 4.8: Period 3.5 filter order comparison

sults, so we can affirm that a unique 70-th order filter is the one both responding to low order and visible detection enhancement requirements.

4.3 Conclusions

UWB is a technology for transmitting information spread over a large bandwidth sharing spectrum with other users. UWB provides an efficient use of scarce radio bandwidth while enabling both high data rate and wireless connectivity as well as radar and imaging systems. Contactless heart and breath rate detection can be achieved with the use of UWB radar device. Main purposes of such device are non intensive-care patient monitoring, home monitoring and fast disease screening. UWB device for heart and breath rate detection can even implement onboard algorithms for detection in order to present results to users in a very easy way so no technical skill is required. Our test devices were provided by PulsON: two PulsON 220RD UWB radar. We encountered an issue with time synchronization that is very critical in UWB detection techniques, unfortunately it was not possible to test a different UWB device nor we were able to rebuild device kernel to cope with the sync issue. A synchronization algorithm is then developed and tested trying to automatically resynchronized scan comparing MSE against a reference scan. The algorithms did the job but could not fully cope

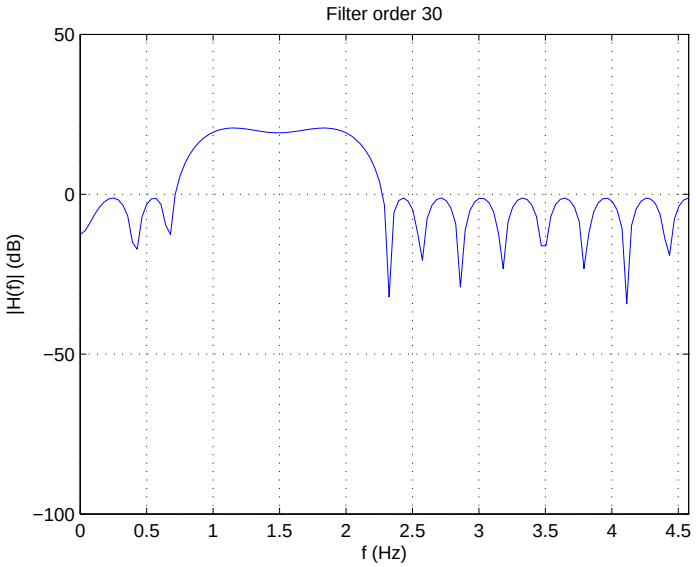

Figure 4.9: Passband 30-th order filter response

with the out-of-sync issue resulting in an big amount of scans not being selected due to very high MSE value mainly caused by half signal set to zero o partially wrapped around. To correctly detect heart and breath rate it is necessary to have a continuous scan set without any gap or interruptions. Moving on a vital data set taken with the previous PulsON device - 210 RD - we analyzed and designed a FIR filter to enhanced heart beat period detection. The filter is a pass band that cuts everything outside average healthy adult heart rate range of $50 - 120$ bpm that is $0.8Hz - 2Hz$. Heart rate detection is then performed with three of the most well known period detection algorithm families: Welch algorithm, MUSIC algorithm and AMDF technique. Beside these, a new maximum likelihood technique is introduced. A comparison between all these algorithms shows Low Complexity Maximum Likelihood as the best performing without any signal processing. After applying the previously designed filter we have an overall improvement except for PWELCH.

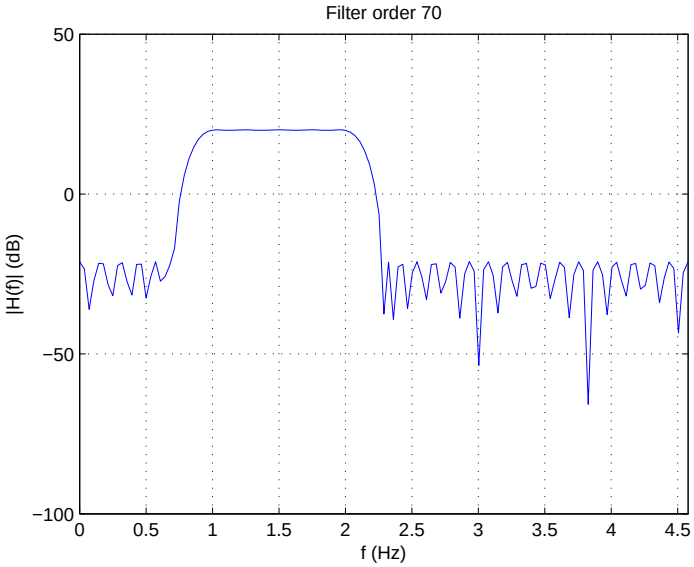

Figure 4.10: Passband 70-th order filter response

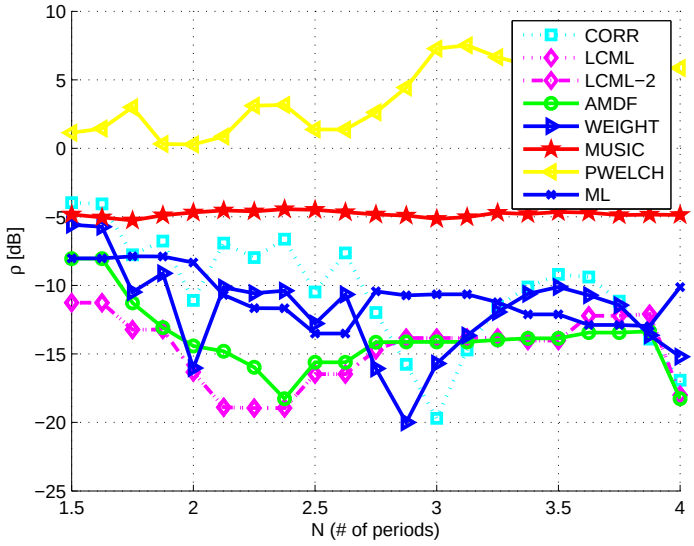

Figure 4.11: Normalized MSE of the estimated heart beat period as a function of N/P. Experimental result. 30-th order filter applied.

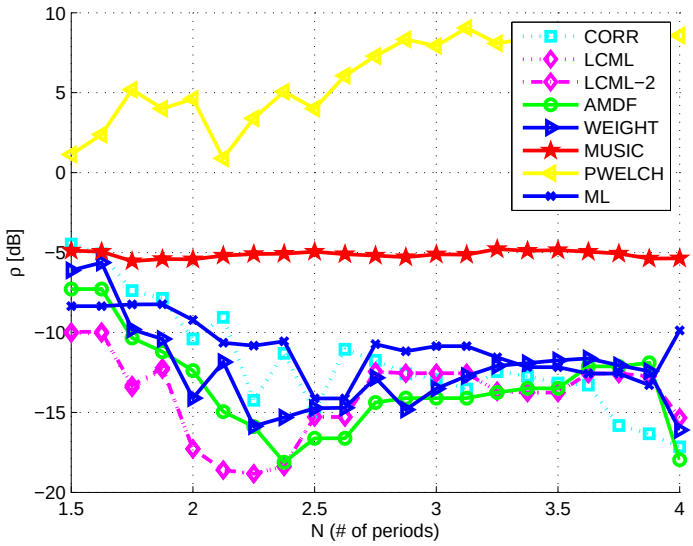

Figure 4.12: Normalized MSE of the estimated heart beat period as a function of N/P. Experimental result. 70-th order filter applied.

Chapter 5

Conclusions

Our aim was to detect vital signs, especially heart beat, in a contactless setup using ultra wide band devices. We realized a measurement scenario with two UWB PulsON 220RD UWB radar. The target is supposed to be still or sitting at a known d_T distance facing the radar and breathing normally. Unfortunately our devices showed poor synchronization capabilities and most of the scans came out of synchronization. First attempts to solve the issue via the provided software were unsuccessful, since no sync parameter is user tunable. We then moved to analyze the source code of the host application running on PC, even this attempt was unsuccessful, no parameter or comment referring to synchronization. At last we took a look at the kernel API but again there was nothing related to signal synchronization.

So, we realized a MATLAB script to batch resynchronize the text saved scan. The *sync_power* algorithms uses the MSE to synchronize the signals against the one with maximum signal power or hand provided. This script did the job but it was not able to cope with the time-variant offset introduced by the PulsON devices. Then, we continued our work on a vital sign dataset taken with the previous PulsON 210 RD version that seemed unaffected by the out-of-sync issue. Background noise subtraction technique is applied to data from radar to remove all the unwanted static reflection caused by other presence in the test area. Once the signal is "clean" we need to detect, if any, its period. Four of the most well-known period estimation algoritms are used: AMDF, MUSIC, WELCH and a new low complexity version of the ML. Performance tests, in terms of normalized MSE, provide that ML is the one best performing. In our case of vital signs

monitoring we known that the signal is the sum of breathing and heart beating. We wanted next to focus our attention on the weaker contributor, that is the signal by heart beating, by filtering out the breathing contribution. The expected heart beating range, for an healthy target is $80 - 100$ bpm so a filter is designed to attenuate everything outside the $0.8Hz - 1.2Hz$ and enhance the inside. An extensive analysis is done to find the best performing low order filter, taking into account that the vital sign dataset has only 118 samples. We discovered that some detection algorithms perform best in $20 - 40$ filter order range while others in $60 - 80$. Two filter are designed, one with order 30 and the other with order 70 this to get the best from each period estimator. WEIGHT and CORR show improvement with the 30-th order filter while LC and LCML achive better result with the 70-th order filter. AMDF performance with 30-th or 70-th order filter are more or less the same. The idea to design two filters for difference period detection algorithm performance achievement did not give the expected great improvement results, so we can argue that a unique 70-th order filter is the one both responding to low order and best detection enhancement requirements.

Bibliography

[1] X. Yong, L. Yinghua, Z. Hongxin, and W. Yeqiu, "An overview of ultra-wideband technique application for medial engineering," *IEEE/ICME International Conference on Complex Medical Engineering(CME)*, May 2007.

[2] R. Cager, D. LaFlame, and L. Parode, "Orbiter ku-band integrated radar and communications subsystem," *IEEE Transactions on Communications*, vol. 26, no. 11, pp. 1604–1619, Nov 1978.

[3] F. C. C. (FCC), "Revision of part 15 of the commission's rules regarding ultra-wideband transmission systems," April 22, 2002.

[4] U. N. I. of Healt, "Sudden infant death syndrome (sids)," http://www.nichd.nih.gov/health/topics/sudden_infant_death_syndrome.cfm.

[5] E. M. Staderini, "Uwb radars in medicine," *IEEE Aerospace and Electronic Systems Magazine*, vol. 17, 2002.

[6] A. Guyton and J. Hall, *Textbook of Medical Physiology*. Saunders, 2005.

[7] E. Conte, "Multiuser mimo downlink systems with limited feedback and remote sensing of vital signs," Ph.D. dissertation, University of Padua, 2010.

[8] V. Novak, P. Novak, J. de Champlain, A. Le Blanc, R. Martin, and R. Nadeau, "Influence of respiration on heart rate and blood pressure fluctuations," *Journal of Applied Physiology*, vol. 74, no. 2, 1993.

[9] C. Gabriel, "A compilation of the dielectric properties of body tissues at rf and microwave frequencies," April 22, 2002.

[10] G. Varotto and E. M. Staderini, "A 2d simple attenuation model for em waves in human tissues: Comparison with a fdtd 3d simulator for uwb medical ra-

dar," *Proceedings of 2008 IEEE international conference on ultra-wideband*, vol. 3, 2008.

[11] G. Kang and O. P. Gandh, "Effect of dielectric properties on the peak 1- and 10-g sar for 802.11 a/b/g frequencies 2.45 and 5.15 to 5.85 ghz," *IEEE transactions on electromagnetic compatibility*, vol. 46, May 2, 2004.

[12] G. Ossberger, T. Buchegger, E. Schimback, A. Stelzer, and R. Weigel, "Non-invasive respiratory movement detection and monitoring of hidden humans using ultra wideband pulse radar," *Proc. IEEE Joint UWBST and IWUWBS 2004*, May 18-21, 2004.

[13] A. Nezirovic, A. G. Yarovoy, and L. P. Ligthart, "Experimental verification of human being detection dependency on operational uwb frequency band," *Proc. 2007 IEEE ICUWB*, Sept. 24-26, 2007.

[14] C. Bilich, "A simple fdtd model to asses the feasibility of heart beat detection using commercial uwb communication devices," 2007.

[15] S. Bevaqua, "I campi elettromagnetici," http://www.ericsson.com/it/docs/campielettromagnetici.pdf.

[16] H. G. Schantz, "Bottom fed planar elliptical uwb antennas," *Ultra Wideband Systems and Technologies, 2003 IEEE Conference on*, 16-19 Nov. 2003.

[17] R. Moresco, *Lezioni di Algebra Lineare e Geometria.* Edizioni Progetto Padova, 2003.

[18] N. Benvenuto, R. Corvaja, T. Erseghe, and N. Laurenti, *Communication Systems.* Wiley, 2006.

[19] P. Welch, "The use of fast fourier transform for the estimation of power spectra: A method based on time averaging over short, modified periodograms," *IEEE Transactions on Audio and Electroacoustics*, vol. 15, Jum. 1967.

[20] R. Schmidt, "Multiple emitter location and signal parameter estimation," *IEEE Trans. Antennas Prop.*, vol. 34, Mar. 1986.

[21] V. F. Pisarenko, "The retrieval of harmonics from a covariance function," *Geophysical Journal of the Royal Astronomical Society*, vol. 33, 1973.

[22] M. Ross, H. Shaffer, A. Cohen, R. Freudberg, and H. Manley, "Average magnitude difference function pitch extractor," *IEEE Transactions on Acoustics, Speech and Signal Processing*, vol. 22, Oct. 1974.

[23] W. Zhang, G. Xu, and Y. Wang, "Pitch estimation based on circular amdf," *Acoustics, Speech, and Signal Processing, 2002. IEEE International Conference on*, vol. 1, 2002.

[24] E. Conte, A. Filippi, and S. Tomasin, "Ml period estimation with application to vital sign monitoring," *IEEE*, 2010, submitted.

[25] H. Kobayashi and T. Shimamura, "A weighted autocorrelation method for pitch extraction of noisy speech," *Acoustics, Speech, and Signal Processing, 2000. IEEE International Conference on*, 2000.

[26] S. Standring, *Gray's Anatomy Edition 39.* Churchill Livingstone.

[27] M. B. Priestley, *Spectral Analysis and Time Series.* Academic Press, 1981, vol. I.

[28] L. Rabiner, M. Chang, R. A.E., and C. McGonegal, "A comparative performance study of several pitch detection algorithms," *IEEE Trans. Acoustics, Speech and Signal Proc.*, vol. ASSP-24, Oct, 1976.

[29] B. Quinn and E. Hannan, *The estimation and tracking of frequency.* Cambridge Univ. Press, 2001.

[30] M. Ross, H. Shaffer, A. Cohen, R. Freudberg, and M. H.J., "Average magnitude difference function pitch extractor," *IEEE Trans. Acoustics, Speech and Signal Proc.*, vol. ASSP-22, Oct, 1974.